On the dissociation pathways of copper complexes relevant as PET imaging agents

Rocío Uzal-Varela [a], Véronique Patinec [b], Raphaël Tripier [b], Laura Valencia [c], Marcelino Maneiro [d], Moisés Canle [a], Carlos Platas-Iglesias [a], David Esteban-Gómez [a,*], Emilia Iglesias [a,*]

[a] Centro de Investigacións Científicas Avanzadas (CICA) and Departamento de Química, Facultade de Ciencias, Universidade da Coruña, 15071 A Coruña, Galicia, Spain
[b] Univ Brest, UMR-CNRS 6521 CEMCA, 6 avenue Victor le Gorgeu, 29238 Brest, France
[c] Departamento de Química Inorgánica, Universidade de Vigo, Facultad de Ciencias, 36310 Pontevedra, Spain
[d] Departamento de Química Inorgánica, Universidade de Santiago de Compostela, Facultade de Ciencias, 27002 Lugo, Spain

ARTICLE INFO

ABSTRACT

Several bifunctional chelators have been synthesized in the last years for the development of new ^{64}Cu-based PET agents for *in vivo* imaging. When designing a metal-based PET probe, it is important to achieve high stability and kinetic inertness once the radioisotope is coordinated. Different competitive assays are commonly used to evaluate the possible dissociation mechanisms that may induce Cu(II) release in the body. Among them, acid-assisted dissociation tests or transchelation challenges employing EDTA or SOD are frequently used to evaluate both solution thermodynamics and the kinetic behavior of potential metal-based systems. Despite of this, the Cu(II)/Cu(I) bioreduction pathway that could be promoted by the presence of bioreductants still remains little explored. To fill this gap we present here a detailed spectroscopic study of the kinetic behavior of different macrocyclic Cu(II) complexes. The complexes investigated include the cross-bridge cyclam derivative [Cu(CB-TE1A)]$^+$, whose structure was determined using single-crystal X-ray diffraction. The acid-assisted dissociation mechanism was investigated using HClO$_4$ and HCl to analyse the effect of the counterion on the rate constants. The complexes were selected so that the effects of complex charge and coordination polyhedron could be assessed. Cyclic voltammetry experiments were conducted to investigate whether the reduction to Cu(I) falls within the window of common bioreducing agents. The most striking behavior concerns the [Cu(NO2Th)]$^{2+}$ complex, a 1,4,7-triazacyclononane derivative containing two methylthiazolyl pendant arms. This complex is extremely inert with respect to dissociation following the acid-catalyzed mechanism, but dissociates rather quickly in the presence of a bioreductant like ascorbic acid.

1. Introduction

Positron emission tomography (PET) is an important technique in medical diagnosis that uses a radionuclide that decays by emitting a positron (β^+), which subsequently travels a short distance *in vivo* until it is annihilated by collision with an electron. This generates nearly coincident γ-rays (180°) that can be registered by an external detector, providing high-resolution images of the body [1,2].

The most widely used PET agent is ^{18}F-fluorodeoxyglucose, a glucose analogue that is efficiently taken up by aggressive tumors [3]. However, several radiometals have also been the subject of intense research efforts in the last decades, notably the ^{68}Ga- and ^{64}Cu-nuclides [4–6]. Several ^{64}Cu-based PET agents are currently in clinical trials, and further developments in this field are expected to come in the next years [4,7]. The human studies performed in this last decade focused mainly in the use of bifunctional chelators that hold the radioactive element and are linked to a targeting moiety, which directs the probe to the desired target *in vivo* [8–11].

Coordination chemistry plays a crucial role in designing an appropriate ligand for ^{64}Cu-nuclide complexation [12,13], as delivering the ^{64}Cu-nuclide to specific targets *in vivo* requires complexation of the radiometal with suitable chelators [14]. In addition, an optimal chelator should afford highly stable complexation to avoid or minimize the amount of the ^{64}Cu-nuclide released *in vivo*. The high sensitivity of PET requires very small amounts of the ^{64}Cu-nuclide to be injected. Thus, chemical toxicity is most likely not a relevant problem. Indeed, [64]CuCl_2 has been successfully used for *in vivo* imaging of both animal models and human subjects [15,16]. However, the release of the ^{64}Cu-nuclide from the chelator introduces a background signal that decreases the signal to noise ratio at the target tissue [17]. Therefore, it is important to design chelators that match the coordination chemistry of copper, so that stable and inert complexes are obtained [18].

Derivatives of the macrocyclic ligand H_4DOTA, such as the FDA approved ^{64}Cu-DOTATATE [19], are probably the most widely used for *in vivo* studies (for instance with ^{64}Cu and ^{68}Ga), most likely because the synthetic technology for incorporating targeting units is well developed [20]. However, the dissociation of H_4DOTA derivatives *in vivo* has been demonstrated [21]. The family of cyclam chelators functionalized with different pendant arms, including carboxylates, [22–26] phosphonates [27–29] and picolinates [30–33] was found to be better suited for stable
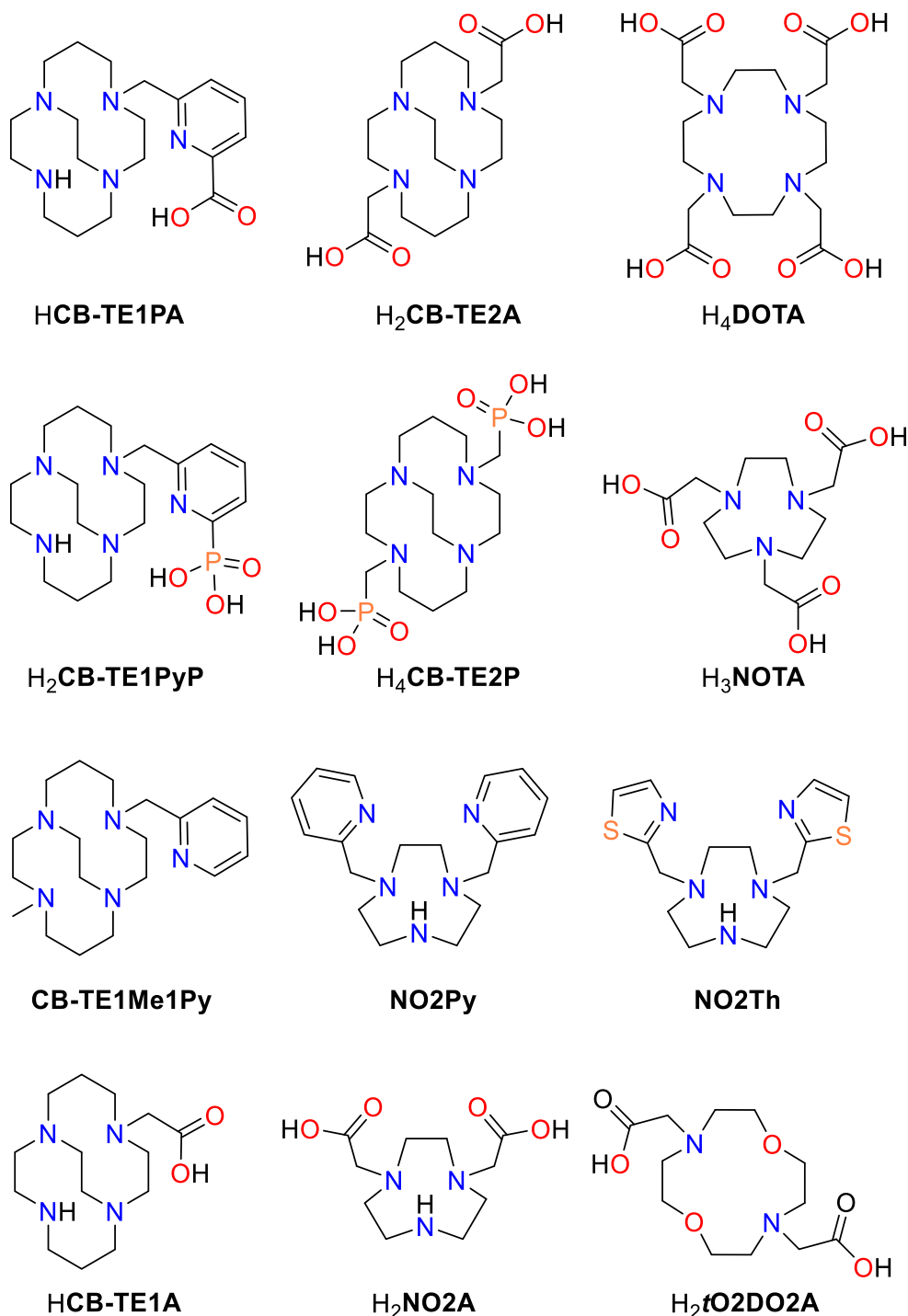
Scheme 1. Ligands discussed in this work.

Cu(II) complexation than cyclen derivatives, less suited for small metal ions. Increasing the rigidity of the cyclam platform by incorporating a bridging unit (i. e. H$_2$CB-TE2A [34–40], H$_4$CB-TE2P [41], HCB-TE1PA [42] and H$_2$CB-TE1PyP [43], Scheme 1) yields particularly inert Cu(II) complexes, although radiolabeling often requires high temperatures that are incompatible with certain sensitive targeting moieties. Radiolabeling is generally faster in the case of phosphonate derivatives compared to the carboxylate analogues [41]. When suitably *N*-functionalized, the triazacyclononane platform was also proved to be very useful for the development of copper-based radiopharmaceuticals, in particular H$_3$NOTA derivatives [21,44]. Other families of ligands with good properties for Cu(II) complexation include bispidine [45–47] and sarcophagine [48,49] derivatives.

The dissociation of copper complexes *in vitro* is generally assessed by investigating their acid-catalyzed dissociation, generally using high acid concentrations [50]. Other potential dissociation pathways may involve transmetallation *in vivo* to proteins such as albumin in blood or superoxide dismutase in the liver [18,51,52]. Furthermore, it has been suggested that the reduction of Cu(II) to Cu(I) and subsequent decomplexation may represent an efficient pathway for complex dissociation [53]. Thus, different authors recommended to shift the reduction potential of the Cu(II) complex below the threshold for bioreductants (−0.4 V *vs* NHE) [54]. Furthermore, the lack of reversibility of the cyclic voltammogram has been correlated to a higher probability of decomplexation upon reduction [55,56]. The dissociation of Cu(II) thiosemicarbazone complexes such as Cu-ATSM in hypoxic tissues is well documented [57–59]. However, no clear evidence for dissociation following the Cu(II)/Cu(I) bioreduction pathway was obtained for other Cu(II) complexes.

In this work, we provide a detailed investigation of the kinetic inertness of the Cu(II) complexes with three pentadentate chelators: HCB-TE1A, NO2Py and NO2Th (Scheme 1). The HCB-TE1A ligand belongs to the family of cross-bridged derivatives that are generally very inert and display rather negative reduction potentials. The Cu(II) complex with NO2Th was investigated recently by some of us, and was found to be very inert under acidic conditions [60]. The [Cu(NO2Th)]$^{2+}$ complex displays a reversible cyclic voltammogram with a redox potential for the Cu(II)/Cu(I) pair of −0.25 V (*vs* NHE in 0.1 M LiClO$_4$). A bifunctional derivative conjugated to a bombesin antagonist peptide was also found to be very inert *in vitro* [61]. The [Cu(NO2Py)]$^{2+}$ complex is structurally related to [Cu(NO2Th)]$^{2+}$, as demonstrated by the comparison of the corresponding crystal structures [60,62]. This complex was investigated here to evaluate the potential ability of the soft sulfur atoms of NO2Th to stabilize the Cu(I) complex. The potential dissociation of the complexes in strong acidic media was investigated using spectrophotometric measurements. To assess the effects of complex charge and coordination number, we also investigated the acid-catalyzed dissociation of the neutral [Cu(NO2A)] and [Cu(tO2DO2A)] complexes, which contain five- and six-coordinated Cu(II) ions, respectively [63]. We also report the characterization of the complexes using cyclic voltammetry experiments. The dissociation of the complexes in the presence of ascorbate as reducing agent was analysed in detail. Finally, we also report the X-ray structure of the Cu(II) complex with HCB-TE1A.

2. Experimental

2.1. Materials

The syntheses of [Cu(NO2Th)](ClO$_4$)$_2$ and [Cu(NO2Py)](ClO$_4$)$_2$ were described previously [60,64]. The NO2Py ligand was obtained following a previously reported procedure [65]. The HCB-TE1A ligand was prepared following the method described by Archibald and collaborators [66]. H$_2$NO2A was obtained by hydrolysis of the commercially available *tert*-butyl ester precursor using trifluoroacetic acid. [Cu(CB-TE1A)](CF$_3$SO$_3$) and [Cu(NO2A)] complexes were prepared by

reaction of the corresponding ligand and Cu(CF$_3$SO$_3$)$_2$ in *n*-butanol. All other chemicals were obtained from commercial sources. Solvents were of reagent grade and used without further purification.

2.2. General methods

Elemental analyses were carried out on a ThermoQuest Flash EA 1112 elemental analyser. High resolution electrospray-ionization time-of-flight ESI-TOF mass spectra were recorded in the positive mode using a LTQ-Orbitrap Discovery Mass Spectrometers coupled to Thermo Accela HPLC or LC-Q-q-TOF Applied Biosystems QSTAR Elite spectrometer in the positive mode. IR spectra were recorded using a Thermo Scientific FT-IR Nicolet iS 10 spectrophotometer equipped with an attenuated total reflectance (ATR) accessory (Thermo Scientific Smart iTR). ^{1}H and ^{13}C NMR spectra were recorded at 25 °C on Bruker Avance 300 and Bruker Avance 500 spectrometers.

2.3. Synthesis

2-(1,4,8,11-tetrabicyclo[6.6.2]hexadecane-4-yl)acetic acid (HCB-TE1A) was isolated as a bromide salt. Elem. Anal. Calcd for C$_{14}$H$_{30}$Br$_2$N$_4$O$_2$: C, 37.7; H, 6.8; N, 12.6%. Found: C, 38.4; H, 6.9; N, 12.6%. MS-ESI$^+$, *m/z* (%BPI): [L + H]$^+$, 285.2 (100%). δ_H (solvent D$_2$O, 500 MHz, 298 K, pD: 3): 4.85 (d, 1H), 3.72 (m, 1H), 3.75–3.10 (m, 12H), 2.96 (m, 5H), 2.80–2.50 (m, 4H), 2.40 (m, 2H), 1.73 (m, 2H). δ_C (solvent D$_2$O, 125.8 MHz, 298 K, pD: 3): 171.3, 58.0, 57.7, 57.6, 55.9, 55.5, 53.9, 49.4, 48.6, 48.3, 47.1, 41.5, 19.2, 18.2. IR (cm^{-1}): 3398, ν(N—H), 1624 ν(C=O).

2,2′-(1,4,7-triaza-1,4-diyl)diacetic acid (H$_2$NO2A). The synthesis of the ligand was achived by acid hydrolysis of the *tert*-butyl groups of commercially available NO2A(O^{t}Bu)$_2$ (0.1261 g, 0.35 mmol) in refluxing HCl 6 M (20 mL) over a period of 16 h. The solvent was removed in a rotary evaporator and water (3 mL) was added. The solvent was again evaporated and this process was repeated twice to remove most of the acid. Finally a solution of the ligand in water (3 mL) was lyophilized. The ligand was isolated as a hydrated chloride salt. Yield 96%. Elem. Anal. Calcd for C$_{10}$H$_{19}$N$_3$O$_4$·3(HCl)·1.5(H$_2$O): C, 31.5; H, 6.6; N, 11.0%. Found: C, 31.7; H, 6.4; N, 10.7%. MS-ESI$^+$, *m/z* (%BPI): [L + H]$^+$, 246.1 (100%). δ_H (solvent D$_2$O, 400 MHz, 298 K, pD = 0.8): 4.01 (s, 4H), 3.60–3.55 (m, 8H), 3.42 (s, 4H). δ_C (solvent D$_2$O, 125.8 MHz, 298 K, pD = 0.8): 172.3, 56.7, 51.1, 50.4, 43.0. IR (cm^{-1}): 3355 ν(N—H), 1729 ν(C=O).

General procedure for the preparation of [Cu(CB-TE1A)](CF$_3$SO$_3$) and [Cu(NO2A)]. A solution of the corresponding ligand (HCB-TE1A, 0.140 mmol; H$_2$NO2A, 0.318 mmol) in *n*-butanol (6 mL) in the presence of DIPEA (6 equivalents) was purged with an argon flow. Afterwards, solid Cu(CF$_3$SO$_3$)$_2$ (1 equivalent) was added and dissolved with the assistance of an ultrasound bath. The reaction was maintained at 90 °C for 22 h and then stopped and allowed to cool to room temperature. Blue crystals or a blue precipitate were formed, which were isolated by filtration in both cases.

[Cu(CB-TE1A)] (CF$_3$SO$_3$). Blue crystals. Yield: 0.045 g, 66%. Elem. Anal. Calcd for C$_{15}$H$_{27}$CuF$_3$N$_4$O$_5$S: C, 36.3; H, 5.5; N, 11.3%. Found: C, 36.3; H, 5.4; N, 11.2%. MS-ESI$^+$, *m/z* (%BPI): [CuL]$^+$, 346.1 (31%). IR (cm^{-1}): 3351 ν(N—H), 1612 ν(C=O).

[Cu(NO2A)]. Blue solid. Yield: 0.073 g, 75%. Elem. Anal. Calcd for C$_{10}$H$_{17}$CuN$_3$O$_4$·2H$_2$O: C, 35.0; H, 6.2; N, 12.3%. Found: C, 34.9; H, 6.1; N, 12.4%. MS-ESI$^+$, *m/z* (%BPI): [Cu(L + H)]$^+$, 307.1 (100%), [CuL + Na]$^+$, 329.0 (100%), [2(CuL) + H]$^+$, 613.1 (46.1%), [2(CuL) + Na]$^+$, 635.1 (84.2%). IR (cm^{-1}): 3299 ν(N—H), 1613 ν(C=O).

2.4. Kinetic experiments

Kinetics of dissociation of the CuL complex in acid conditions (HCl or HClO$_4$) were investigated by following the ligand absorption bands (wavelength around 300 nm) using the acid concentration in high excess

relative to the complex concentration (10^{-4} to 10^{-5} M, depending on the ligand). Slow reactions were monitored by a Kontron-Uvikon 942 UV–vis spectrophotometer at 25 °C and 1 cm path-ligth quartz cuvette, with the CuL complex being the last reagent added to the sample reaction.

The fast reactions were monitored on a Bio-Logic SFM-20 stopped-flow system interfaced with a computer and operated by a Bio-Kine 32 (v4.51) software that controls both the data acquisition and analysis. One syringe contained the CuL complex at the same ionic strength that the acid introduced in the second syringe. Each experiment was taken in triplicate.

The dissociation kinetics in neutral medium were studied in phosphate buffer of varying pH in the presence of ascorbic acid, which is able to reduce Cu(II) to Cu(I), and neocuproine that is a Cu(I) scavenger due to 1:2 complex formation ([Cu(NC)$_2$]$^+$). The reactions were monitored by conventional spectroscopy following the increase in absorbance at 454 nm due to Cu(I)-neocuproine complex ($\varepsilon \approx 7500$ M$^{-1} \cdot$cm^{-1}) and keeping the ratio [neocuproine]/[CuL] higher than *ca.* 2.5. Neocuproine was added upon dissolution in a small amount of dioxane (%*v*/*v* dioxane/water = 1.0–3.3% in the final solutions used for kinetics experiments).

In every case, experiments were performed under pseudo-first order conditions. Absorbance (A) *versus* time (t) curves were appropriately fitted by a first-order integrated rate Eq. (1), with A_o, A_t, and A_∞ being the absorbance values at times zero, *t*, and at the end of the reaction, and k_o is the calculated pseudo-first order rate constant.

$$A_t = A_\infty + (A_o - A_\infty) \cdot e^{-k_o t} \tag{1}$$

2.5. Cyclic voltammetry

Cyclic voltammetry experiments were carried out using an Autolab PGSTAT101 potentiostat working with a three-electrode configuration. A glassy carbon disc (Metrohm 6.1204.000) was used as the working electrode. The surface of the electrode was polished before each measurement using α-Al$_2$O$_3$ (0.3 μm) and washed with distilled water. A Ag/AgCl reference electrode filled with 3 M KCl (Metrohm 6.0728.000) was used as the reference electrode, while a Pt wire was used as the counter electrode. The solutions of the complexes (1.7–1.9 × 10^{-3} M) containing 0.15 M NaCl as supporting electrolyte were deoxygenated by bubbling N$_2$ prior each measurement.

2.6. X-ray diffraction

A single crystal of [Cu(CB-TE1A)](CF$_3$SO$_3$) was analysed by X-ray diffraction and a summary of the crystallographic data and the structure

refinement parameters is reported in Table 1. A Bruker D8 Venture diffractometer with a Photon 100 CMOS detector was used to collect crystallographic data at 100 K. Mo-Kα radiation (λ = 0.71073 Å) was generated by an Incoatec high brillance microfocus source equipped with Incoatec Helios multilayer optics. The software APEX3 [67] was used for collecting frames of data, indexing reflections, and the determination of lattice parameters, SAINT [68] for integration of intensity of reflections, and SADABS [69] for scaling and empirical absorption correction. The structure was solved by dual-space methods using the program SHELXT [70]. All non-hydrogen atoms were refined with anisotropic thermal parameters by full-matrix least-squares calculations on F^2 using the program SHELXL-2014 [71]. Hydrogen atoms were inserted at calculated positions and constrained with isotropic thermal parameters.

2.6.1. Accession codes

CCDC 2160376 contains the supplementary crystallographic data for this paper. These data can be obtained free of charge *via* www.ccdc.cam.ac.uk/data_request/cif, or by emailing data_request@ccdc.cam.ac.uk, or by contacting The Cambridge Crystallographic Data Centre, 12 Union Road, Cambridge CB2 1EZ, UK; fax: + 441,223 336,033.

3. Results and discussion

3.1. Crystal structure

The X-ray structure of [Cu(CB-TE1A)](CF$_3$SO$_3$) contains a five-coordinated Cu(II) ion, which is directly bonded to the four nitrogen atoms of the macrocyclic unit and an oxygen atom of the carboxylate pendant arm (Fig. 1). As usually observed for Cu(II) complexes of cross-bridge cyclam derivatives, the macrocycle adopts the typical *cis*-V conformation, with the six-membered chelate rings presenting chair conformations. As a result, the bicyclo[6.6.2] fragments display [2323] conformations according to the nomenclature proposed by Dale [72,73], as observed for most complexes with cross-bridged cyclam derivatives and small metal ions [74–77].

The coordination polyhedron may be described as a distorted trigonal bipyramid, in which the axial positions are defined by N(1) and N(3) [N(1)-Cu(1)-N(3) = 176.45(11)°] and the equatorial plane is delineated by O(1), N(2) and N(4). The presence of the ethylene bridging unit imposes a closed N(2)-Cu(1)-N(4) angle of 87.19(10)° and an open O(1)-Cu(1)-N(2) angle of 148.20(11)°. The third angle of the equatorial plane is relatively close to the ideal value of 120° expected for a trigonal bipyramid [O(1)-Cu(1)-N(4) = 124.58(10)°]. The analysis of

Table 1
Crystallographic data and structure refinement parameters for [Cu(CB-TE1A)](CF$_3$SO$_3$).

Formula	C$_{15}$H$_{27}$CuF$_3$N$_4$O$_5$S
MW	496.00
Crystal system	Monoclinic
Space group	P2$_1$/c
a/Å	8.7005(3)
b/Å	14.9861(4)
c/Å	15.0251(5)
β/deg	98.5450(10)
V/Å^3	1937.32(11)
Z	4
D$_{calc}$ g/cm^3	1.701
μ/mm^{-1}	1.300
R$_{int}$	0.0417
R$_1$ [a]	0.0504
wR$_2$ [b] [all data]	0.1734

[a] R$_1$ = Σ||F$_o$|-|F$_c$||/Σ|F$_o$|.
[b] wR$_2$ = {Σ[w(||F$_o$|^2-|F$_c$|^2|)^2]/Σ[w(F$_o^4$)]}$^{1/2}$.
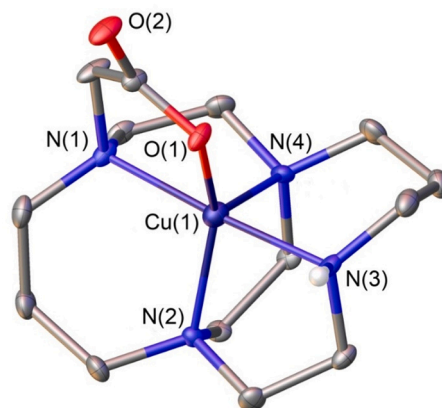
Fig. 1. X-ray crystal structure of the [Cu(CB-TE1A)]$^+$ cation present in crystals of [Cu(CB-TE1A)](CF$_3$SO$_3$). Hydrogen atoms are omitted for simplicity. The ORTEP plot is at the 50% probability level. Bond distances (Å): Cu(1)-N(1), 2.023(3); Cu(1)-N(2), 2.045(3); Cu(1)-N(3), 1.999(3); Cu(1)-N(4), 2.176(3); Cu(1)-O(1), 1.940(2).

the coordination polyhedron using shape measures [S(A)] confirms that the coordination polyhedron is closer to a trigonal bipyramid [S(A) = 2.85] than to a square pyramid [S(A) = 3.38] [78,79].

The carboxylate oxygen atom provides a rather strong coordination to the Cu(II) ion [Cu(1)-O(1) = 1.940(2) Å]. Indeed, the six-coordinated analogue [Cu(CB-TE2A)] shows a short Cu—O bond of 1.998 Å and a long distance of 2.327 Å. The latter complex also shows an elongated Cu—N bond of 2.224 Å, as a result of the Jahn-Teller distortion [80]. The [Cu(CB-TE1A)]$^+$ complex presents three short Cu—N distances (~2.00–2.05 Å) and a fourth longer Cu(1)-N(4) bond of 2.176(3) Å. Thus, the five-coordinate [Cu(CB-TE1A)]$^+$ complex presents a more compact structure than the six-coordinate Jahn-Teller distorted [Cu(CB-TE2A)] analogue. A five-coordinated Cu(II) complex with a cross-bridge derivative containing a pyridyl pendant arm (CB-TE1Me1Py, Scheme 1) presents significantly longer Cu—N distances involving the amine N atoms (2.05–2.14 Å) [77].

3.2. Stability in acidic conditions

3.2.1. Effect of the counterion on the rate constants

The potential dissociation of the [Cu(CB-TE1A)]$^+$ complex was investigated in acidic solution with HCl concentrations in the range 18–162 mM. The absorption spectrum of the complex shows a weak absorption band at 598 nm (ε ~ 93 M^{-1} cm^{-1}) associated to metal *d-d* transitions, as well as a more intense absorption at 260 nm (ε ~ 3900 M^{-1} cm^{-1}, Fig. S9, Supporting Information). The absorption spectrum does not change with time over a period of weeks, indicating that the complex does not dissociate under these conditions. Negligible changes in the absorption spectrum were observed in 2.5 M HCl over a period of

48 h, for a period of 3 h in 2.91 M HCl at 80 °C, or even heating a 5 M HCl solution of the complex at 87 °C. These results indicate that the [Cu(CB-TE1A)]$^+$ complex is particularly resistant to dissociation under acidic conditions (Fig. S10, Supporting Information). The [Cu(CB-TE2A)] complex displays a similar kinetic inertness, with no dissociation observed in 2.24 M HCl at 80 °C over a period of several hours, or even heating a 5 M HCl solution of the complex at 87 °C (Fig. S11, Supporting Information). Thus, both the CB-TE2A^{2-} and CB-TE1A$^-$ ligands form similarly inert complexes with Cu(II), in spite of the lower denticity of the latter. This behavior is in sharp contrast with that of the [Cu(CB-TE1Me1Py)]$^{2+}$, which experiences fast dissociation in acidic conditions [77]. The high inertness of [Cu(CB-TE1A)]$^+$ makes this platform very attractive for the preparation of bifunctional chelators by convenient functionalization of the secondary amine N atom. This may represent a clear advantage with respect to [Cu(CB-TE2A)], which requires a more difficult C-functionalization for the preparation of bifunctional derivatives [81].

The behavior of [Cu(NO2Th)]$^{2+}$ and [Cu(NO2Py)]$^{2+}$ in acidic conditions was investigated by following the ligand absorption bands with maxima at 240 (ε ~ 9400 M^{-1} cm^{-1}) and 260 nm (ε ~ 12,200 M^{-1} cm^{-1}), respectively. Given that chloride is present at rather high concentrations *in vivo* (~0.10 M in human blood plasma) [82], we performed kinetic experiments using both HClO$_4$ and HCl, so that the effect of the presence of the coordinating Cl$^-$ anion can be analysed. The concentration of acid was varied in the range 0.12–3.0 M (HClO$_4$) and 0.10–2.6 M (HCl). The absorption spectra of both [Cu(NO2Th)]$^{2+}$ and [Cu(NO2Py)]$^{2+}$ experienced changes with time in the presence of HClO$_4$ that could be followed using conventional spectrophotometric measurements (Fig. 2a and b). The time scale of the reaction is faster in the
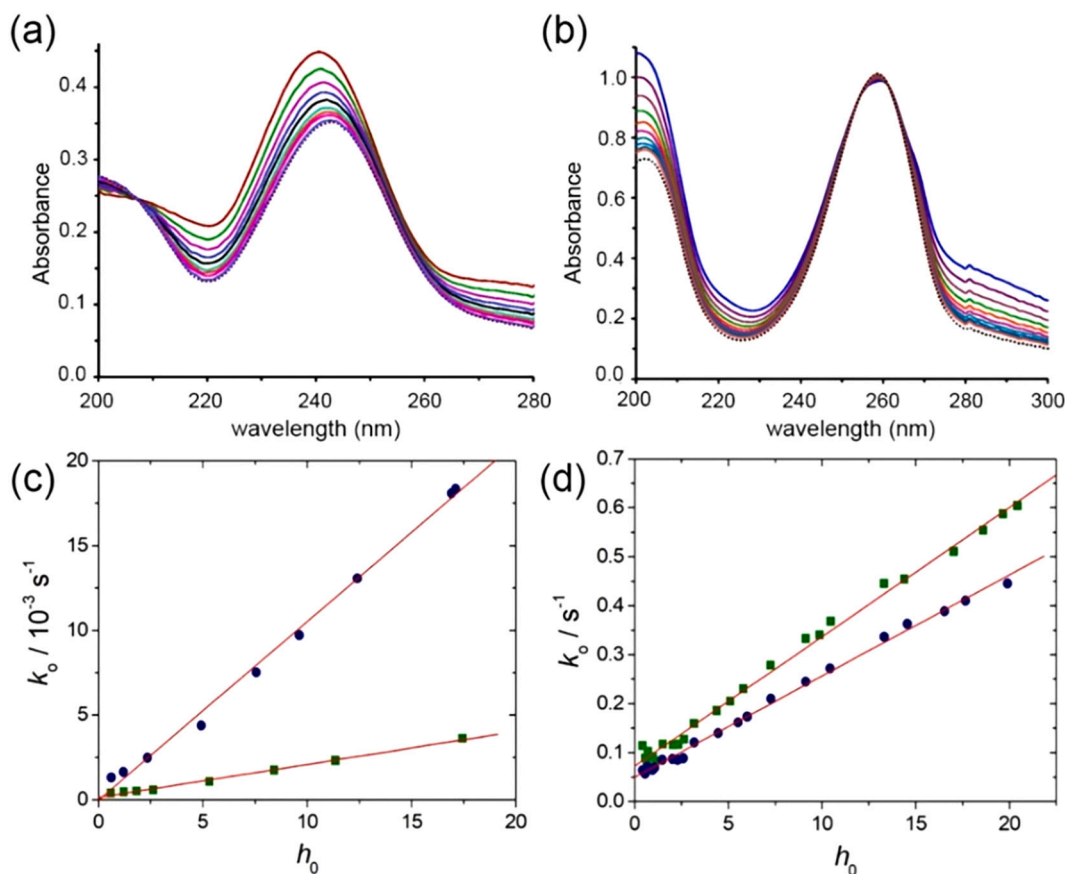
Fig. 2. (a) Absorption spectra of [Cu(NO2Th)]$^{2+}$ (48 μM, [HClO$_4$] = 1.50 M; I = 3.0 M NaClO$_4$) recorded at 3 min intervals. The dotted trace corresponds to the spectrum recorded after 30 min. (b) Absorption spectra of [Cu(NO2Py)]$^{2+}$ (82 μM, [HClO$_4$] = 0.94 M; I = 3.0 M) recorded at 1 min intervals. The dotted trace corresponds to the spectrum recorded after 20 min. (c) and (d) Variation of k_o with the Hammett function, h_o, for [Cu(NO2Th)]$^{2+}$ (■) and [Cu(NO2Py)]$^{2+}$ (●) with I = 3.0 M (NaClO$_4$) (c) or NaCl (d).

presence of HCl, and thus stopped-flow measurements were performed. The ionic strength was maintained constant during the measurements to $I = 3$ M using either $NaClO_4$ or NaCl. The high $[H^+]$ concentration with respect to the concentration of the complex (48 and 82 μM for $[Cu(NO2Th)]^{2+}$ and $[Cu(NO2Py)]^{2+}$, respectively), ensures pseudo-first order conditions throughout the kinetic experiments.

The intensity of the absorption maximum of $[Cu(NO2Th)]^{2+}$ at 240 nm decreases with time upon addition of $HClO_4$ with the concomitant formation of an isosbestic point at 207 nm. For $[Cu(NO2Py)]^{2+}$, the absorption of the pyridyl groups at 260 nm experiences only slight changes with time as an isosbestic point arises at 262 nm (Fig. 2). Similar spectral changes were observed upon addition of HCl. The charge transfer band observed for the two complexes as a shoulder at 270–290 nm decreases in intensity with time, but it does not disappear completely. Furthermore, the solutions retain the characteristic blue color of the complexes, which indicates that no dissociation occurs under the conditions employed for kinetic experiments. This is in agreement with the speciation calculated from the stability constants reported previously for $[Cu(NO2Th)]^{2+}$ in 0.1 M KNO_3, which indicates that complex dissociation requires $[H^+] > 5$ M (Fig. S12, Supporting Information). Furthermore, the presence of chloride anions has a clear effect in accelerating the reactions.

The spectral changes observed in the absorption spectra are thus assigned to a slow protonation of the complex according to Eqs [1,2], where L represents the ligand, k_1 and k_{-1} are the rate constants characterizing the forward and reverse reaction.

$$[CuL]^{2+} + H^+ \underset{k_{-1}}{\overset{k_1}{\rightleftharpoons}} [CuHL]^{3+} \tag{1}$$

$$[CuL]^{2+} + Cl^- \overset{K_x}{\rightleftharpoons} [CuClL]^+$$
$$+$$
$$H^+$$
$$k_{-1} \Big\Updownarrow k_1$$
$$[CuCl(HL)]^{2+} \tag{2}$$
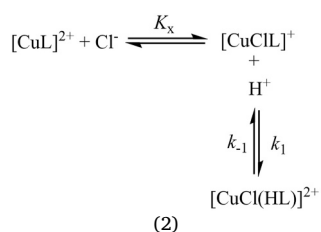
The interaction of $[Cu(NO2Th)]^{2+}$ and $[Cu(NO2Py)]^{2+}$ with Cl^- was investigated by analysing the changes in the *d-d* absorption bands of the complexes at 622 and 613 nm, respectively, that is, under equilibrium conditions for step 1 in Eq. (2), where $K_e = K_X K_1$. The absorption spectrum of $[Cu(NO2Th)]^{2+}$ remains unchanged upon addition of chloride concentrations of up to 0.9 M (Fig. S13, Supporting Information). However, important spectral changes are observed in the *d-*
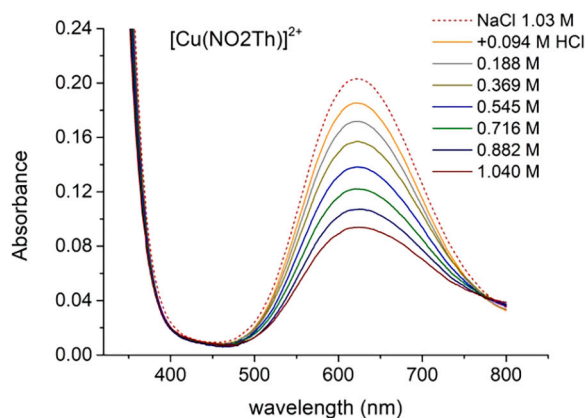
d transitions of both $[Cu(NO2Th)]^{2+}$ and $[Cu(NO2Py)]^{2+}$ upon addition of both HCl and NaCl, with a significant decrease of the intensity of the absorption band and the formation of well defined isosbestic points (Fig. 3, see also Fig. S14, Supporting Information). This indicates that both Cl^- and $[H^+]$ are involved in the reaction, in agreement with Eq. (2), and that most likely chloride is involved in coordination to the metal ion. The *d-d* absorption band of $[Cu(NO2Th)]^{2+}$ is however barely affected by addition of perchloric acid (Fig. S13, Supporting Information), suggesting that the anion is not directly involved in coordination to the metal ion, as would be expected Eq. (1).

The scheme reaction shown in Eq. (2) implies the presence of an equilibrium characterized by a constant K_e, which can be expressed as the product of the protonation constant of the complex K_1 and the equilibrium constant for the coordination of Cl^- to the complex (K_X). Thus, Eq. (3) can be derived from Eq (2), where A_o is the absorbance in the absence of HCl and A_e is the absorbance at the corresponding HCl concentration. This expression can be rearranged in its linear form according to Eqs. (4) and (5). Fig. 3 shows the corresponding linear plots for $[Cu(NO2Th)]^{+2}$ (Fig. S14 presents the data obtained for $[Cu(NO2Py)]^{+2}$). The equilibrium constants obtained for $[Cu(NO2Th)]^{+2}$ using expressions (4) and (5) are in good mutual agreement (Table 2). Interestingly, the $[Cu(CB-TE1A)]^+$ complex also experiences protonation when dissolved in aqueous HCl (0.12–2.91 M, Fig. S15, Supporting Information). However, the observed A_o/A_e values show a linear dependence with $[H^+]$, indicating that the anion is not assisting complex protonation, which may be related to the lower positive charge of the complex.

$$K_e = K_X K_1 = \frac{A_o - A_e}{A_o [Cl^-]_t [H^+]_t} \tag{3}$$

$$A_o/A_e = 1 + K_X K_1 [H^+]_t^2 \tag{4}$$

Table 2
Equilibrium constants [25 °C] obtained for complex protonation in aqueous HCl solution.

	[NaCl]/ M	$[Cu(NO2Th)]^{2+}$	$[Cu(NO2Py)]^{2+}$	$[Cu(CB-TE1A)]^+$
[Complex]/ mM	–	1.63	1.94	1.85
$K_X K_1 / M^{-2}$	0.0^a	0.415 ± 0.02	0.64 ± 0.03	–
$K_X K_1 / M^{-2}$	1.03^b	0.448 ± 0.015	–	–
K_1 / M^{-1}	0.0	–	–	0.120 ± 0.005

^{a} Linearization according to Eq. (4), as in the absence of NaCl $[H^+] = [Cl^-]$.
^{b} Linearization according to Eq. (5).
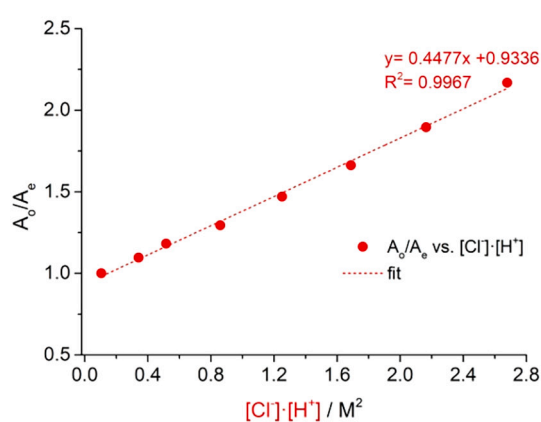
Fig. 3. Left: Spectra of $[Cu(NO2Th)]^{2+}$ (1.63 mM) in 1.03 M of NaCl (dashed red curve) and spectra recorded after the addition (at 5 min interval) of increasing amounts of HCl. Right: Linear increase of the ratio of absorbance readings at 620 nm as a function of the product $[Cl^-]\cdot[H^+]$ according to Eq. (5). (For interpretation of the references to color in this figure legend, the reader is referred to the web version of this article.)

$$A_o/A_e = 1 + K_X K_1 [Cl^-]_t [H^+]_t \tag{5}$$

The rate constants observed for the protonation of $[\text{Cu(NO2Th)}]^{2+}$ and $[\text{Cu(NO2Py)}]^{2+}$ increase linearly with proton concentration in the range $1 < [\text{H}^+] < 3$ M but show deviations from the linear behavior below that range (Fig. S16 Supporting Information). However it is important to take into account that for concentrated solutions of strong acids $[\text{H}^+]$ does not provide an accurate measure of acidity due to variations of the activity coefficients. Instead the acidity of the solution can be measured using the Hammett acidity function H_0 intended to represent the pH of concentrated solutions of strong acids:

$$H_0 = -\log a_{H^+} = -\log h_o \tag{6}$$

Here, a_{H^+} is the proton activity coefficient. The values of $-H_0$ at $I = 3$ M (HClO$_4$ + NaClO$_4$) reported in the literature [83] were used to calculate h_0 for the $[\text{H}^+]$ concentrations used in the kinetic experiments according to (Fig. S17, Supporting Information):

$$h_0 = 4.9291[\text{H}^+] + 0.2899[\text{H}^+]^2 \tag{7}$$

Similarly, the values of h_0 in HCl solutions were calculated from $-H_0$ values reported at $I = 4.8$ M (HCl + NaCl) [84]:

$$h_0 = 4.573[\text{H}^+] + 1.232[\text{H}^+]^2 \tag{8}$$

Plots of the observed rate constants k_o show a linear dependence with h_0 (Fig. 1). Thus, the kinetic data were fitted to the following expression:

$$k_o = k_1 h_0 + k_{-1} \tag{9}$$

In this expression, k_1 and k_{-1} represent the rate constants characterizing the forward (protonation) and reverse (deprotonation) reactions, respectively, which may be assisted by chloride coordination, that is, in HCl aqueous medium the Eq. (9) is $k_o = k_1 K_X h_o + k_{-1}$. The linear fit of the data to Eq. (9) provided the rate constants shown in Table 3 (Fig. 2). The results of the linear fits (Fig. S18, Supporting Information) provide a non negligible y-intercept value for $[\text{Cu(NO2Th)}]^{2+}$ in HClO$_4$, which indicates the presence of a protonation equilibrium in solution characterized by an equilibrium constant $K_1 = k_1/k_{-1}$. This is confirmed by the plots of $[A_o\text{-}A_\infty]$ *versus* $[\text{H}^+]$, which show a saturation behavior typical of equilibrium reactions, as the full protonation of the complex is only achieved at high proton concentrations (Fig. S19, Supporting Information). For $[\text{Cu(NO2Py)}]^{2+}$ the value of the y-intercept was too small to allow for an estimation of k_{-1} and thus the protonation constant. The rate constants obtained upon addition of HCl also show good linearity with h_0 and non negligible y-intercepts, affording the rate constants and equilibrium constants $K_X K_1$ given in Table 3. The values of $K_X K_1$ obtained from kinetic and equilibrium experiments show excellent mutual agreement (see Tables 2 and 3).

The kinetic data show that the $[\text{Cu(NO2Th)}]^{2+}$ and $[\text{Cu(NO2Py)}]^{2+}$ complexes present a similar behavior in the presence of HClO$_4$, but protonation is significantly faster for the latter. The rate constants determined using HClO$_4$ are clearly lower than those obtained in HCl. Furthermore, protonation in HCl is slightly faster for $[\text{Cu(NO2Th)}]^{2+}$

Table 3
Rate and protonation constants [25 °C] obtained for the protonation of [Cu (NO2Th)]$^{2+}$ and [Cu(NO2Py)]$^{2+}$ in HClO$_4$ and HCl solutions.

		[Cu(NO2Th)]$^{2+}$	[Cu(NO2Py)]$^{2+}$
HClO$_4$[a]	k_1 [M^{-1} s^{-1}]	$(1.94 \pm 0.06) \times 10^{-4}$	$1.05 \pm 0.02 \times 10^{-3}$
	k_{-1} [s^{-1}]	$(1.66 \pm 0.46) \times 10^{-4}$	very small
	K_1 / M^{-1}	1.17 ± 0.36	–
HCl[b]	$k_1 K_x$ [M^{-2} s^{-1}]	$2.64 \pm 0.04 \times 10^{-2}$	$2.07 \pm 0.03 \times 10^{-2}$
	k_{-1} [s^{-1}]	$7.3 \pm 0.4 \times 10^{-2}$	$5.0 \pm 0.3 \times 10^{-2}$
	$K_X K_1$ / M^{-2}	0.36 ± 0.03	0.41 ± 0.03

[a] $I = 3$ M (HClO$_4$ + NaClO$_4$).
[b] $I = 3$ M (HCl + NaCl).

than for $[\text{Cu(NO2Py)}]^{2+}$. Thus, chloride coordination to the metal ion assists complex protonation, an effect that appears to be more accute for $[\text{Cu(NO2Th)}]^{2+}$. This is likely related to the different degrees of distortion of the square-pyramidal coordination polyhedron, which is more distorted towards a trigonal prism in $[\text{Cu(NO2Py)}]^{2+}$ (32%) than is in $[\text{Cu(NO2Th)}]^{2+}$ (24%) [60,62], as estimated using the approach of Addison [85]. Complex protonation likely occurs on one of the nitrogen atoms of a pendant arm, which does not coordinate to the metal ion upon protonation. The metal coordination environment may be then completed by chloride anions. This is supported by the X-ray structure of a related complex, which displays a uncoordinated protonated thiazol pendant arm and a chloride anion coordinating to the metal ion [61]. The protonation constants determined from kinetic data for $[\text{Cu(NO2Th)}]^{2+}$ and $[\text{Cu(NO2Py)}]^{2+}$ are very similar, in spite of the lower basicity of thiazole compared to pyridine moiety [86].

The positive charge of the $[\text{Cu(NO2Th)}]^{2+}$ and $[\text{Cu(NO2Py)}]^{2+}$ complexes likely make them very resistant to acid-catalyzed dissociation. Indeed, different studies revealed that increasing the positive charge of structurally related macrocyclic complexes resulted in an increased kinetic inertness [87–89]. The half-life time of [Cu (NO2Th)]$^{2+}$ was found to be *ca.* 15 days in 2 M HCl at 90 °C and fast in 5 M HCl at 25 °C [60]. The visible absorption spectra of $[\text{Cu(NO2Th)}]^{2+}$ and $[\text{Cu(NO2Py)}]^{2+}$ recorded in 5 M HCl confirm the complete and instantaneous dissociation of the complexes at 25 °C by the disappearance of the characteristic *d-d* transitions (Fig. S20, Supporting Information).

3.2.2. Effect of the total charge of the complex

To analyse the effect that the charge of the complex has in the acid-catalyzed dissociation mechanism, we turned our attention to the neutral $[\text{Cu(NO2A)}]$ complex. The absorption spectrum of $[\text{Cu(NO2A)}]$ shows an intense absorption band with a maximum at 263 nm that can be attributed to a charge transfer band, and a weaker band at 650 nm due to metal *d-d* transitions. Complex dissociation was initially investigated at low proton concentrations of $[\text{H}^+] < 0.1$ ($I = 0.5$ M NaCl) using conventional spectrophotometric experiments. The dissociation of the complex is only partial under these conditions, as reflected by the dependence of the absorbance at equilibrium (A_e) with $[\text{H}^+]$. Complex dissociation is complete at $[\text{H}^+]$ of ~0.5 M, as evidenced by the spectral variations observed for the *d-d* absorption band (Fig. S21, Supporting Information). The values of A_0/A_e display a linear dependence with $[\text{H}^+]^2$ (Fig. S22), which indicates that complex dissociation occurs through the formation of a diprotonated species according to the following scheme, where L = NO2A^{2-}:

$$\tag{10}$$

Here, a fast protonation process is followed by a rate-determining step involving dissociation of the protonated complex. Considering the definition of the equilibrium constant characterizing the formation of the diprotonated species ($\beta_2 = K_1^H K_2^H$), and that, 1) the absorbance observed at 294 nm is due to the [CuL] complex, as the free Cu(II) does not have significant absorption at this wavelength, and 2) proton concentration is much higher than the concentration of the complex, one can obtain the following expression:

$$\frac{A_0}{A} = 1 + \beta_2 [\text{H}^+]^2 \tag{11}$$

The linear fit of the data afforded $\beta_2 = 469 \pm 1.0$ M^{-2}. This relatively high protonation constant shows that the $[\text{Cu(NO2A)}]$ complex can be

protonated rather easily, which triggers complex dissociation. The X-ray structure of the protonated $[Cu(HNO2A)]^+$ complex was reported. This structure shows that protonation takes place on an oxygen atom of one of the carboxylate groups, which does not coordinate to the metal ion [90].

Complex dissociation was investigated at higher concentrations of H^+ (0.1–1.0 M) with ionic strengths adjusted to 1.0 M with either $NaClO_4$ or NaCl. The acid-catalyzed dissociation of $[Cu(NO2A)]$ is very fast under these conditions, and thus stopped-flow spectrophotometric measurements were used to follow complex dissociation. This is in sharp contrast with the astonishing kinetic inertness of the structurally related $[Cu(NO2Th)]^{2+}$ and $[Cu(NO2Py)]^{2+}$ complexes. Acid addition (HCl or $HClO_4$) induces a very fast decrease of the intensity of the absorption at 294 nm due to complex dissociation. The dissociation rates k_o increase with increasing proton concentration. The rate constants determined for $[Cu(NO2A)]$ in $I = 1.0$ ($HClO_4$ + $NaClO_4$) M display a linear dependence with $[H^+]$, while the results obtained using $I = 1.0$ (HCl + NaCl) M evidence a quadratic dependence with $[H^+]$ (Fig. 4). The kinetic data can be interpreted as the result of mono- and di-protonation equilibrium steps following by complex dissociation Eq. (10).

The kinetic data were thus analysed by Eq. (9), which can be linearized as in Eqs. (12 and 13):

$$k_o = k_1 K_1^H [H^+] + k_2 K_1^H K_2^H [H^+]^2 \qquad (12)$$

$$\frac{k_o}{[H^+]} = k_1 K_1^H + k_2 K_1^H K_2^H [H^+] \qquad (13)$$

In these expressions, k_1 and k_2 are the rate constants characterizing the acid-catalyzed dissociation through formation of mono- or di-protonated intermediates (Table 4). The dissociation of $[Cu(NO2A)]$ was found to be significantly faster when using NaCl to adjust the ionic strength. This result is very relevant for PET applications, as NaCl is in rather high concentration in plasma (0.9% saline, which corresponds to a NaCl concentration of 0.154 M, is isoosmolar to human plasma) [82]. It is likely that Cl^- forms a ternary complex with $[Cu(NO2A)]$, facilitating complex dissociation. The formation of the ternary complex is probably facilitated by the five-coordination of the metal ion by the ligand. The coordination of the chloride anion results in a distorted octahedral environment, where a pronounced Jahn-Teller distortion would enhance the kinetic lability of the system. This situation was previously found when comparing five-coordinated Cu(II) complexes with respect to six-coordinated analogues [91].

3.2.3. Effect of the ligand denticity

To investigate the effect of ligand denticity on acid assisted

Table 4
Rate constants characterizing the acid-catalyzed dissociation of $[Cu(NO2A)]$ and $[Cu(tO2DO2A)]$ at 25 °C using different ionic strengths and half-lives at pH 7.4.

		$[Cu(NO2A)]$[a]	$[Cu(tO2DO2A)]$[b]
$HClO_4$	$k_1 K_1^H$ [$M^{-1} s^{-1}$]	0.754 ± 0.006	65.4 ± 2.2
	$k_2 K_1^H K_2^H$ [$M^{-2} s^{-1}$]	–	983 ± 15
	$\tau_{1/2}$ [h][c]	6414	74
HCl	$k_1 K_1^H$ [$M^{-1} s^{-1}$]	0.91 ± 0.03	69.1 ± 2.4
	$k_2 K_1^H K_2^H$ [$M^{-2} s^{-1}$]	1.02 ± 0.04	1304 ± 16
	$\tau_{1/2}$ [h] [c]	5338	72

[a] $I = 1.0$ M (HCl + NaCl) or ($HClO_4$ + $NaClO_4$).
[b] $I = 0.5$ M (HCl + NaCl) or ($HClO_4$ + $NaClO_4$).
[c] Calculated at pH 7.4.

dissociation mechanism, we have investigated the recently reported $[Cu(tO2DO2A)]$ complex, as the larger size of the macrocyclic unit results in a six-coordinated Cu(II) ion [63]. The dissociation of $[Cu(tO2DO2A)]$ is considerably faster than that of $[Cu(NO2A)]$. This is reflected in the lifetimes ($\tau_{1/2}$) of the complexes at pH 7.4 estimated from the rate constants of the acid-catalyzed dissociation reaction (Table 4). The lifetime of the $[Cu(DOTA)]^{2-}$ complex at pH 7.4 (~2000 h) is significantly longer than that of $[Cu(tO2DO2A)]$ [92,93]. Dissociation of the $[Cu(DOTA)]^{2-}$ complex *in vivo* is well documented [94], and thus the 1,7-diaza-12-crown-4 macrocyclic fragment of $H_2tO2DO2A$ is not well suited for the design of inert Cu(II) complexes. The rate constants measured for $[Cu(tO2DO2A)]$ show a quadratic dependence with $[H^+]$ regardless of the ionic strength (Fig. 4). In the latter case, the presence of Cl^- anions does not have a significant impact in the observed rate constants, confirming that the six-coordinate Cu(II) ion has little tendency to bind to additional ligands such as Cl^- anions. It is worth indicating that the proton-assisted dissociation mechanism in complexes with polyaminopolycarboxylate ligands starts with the protonation of a carboxylate group, which likely remains coordinated to the metal ion [95]. This protonation process triggers a cascade of structural reorganizations, in which the proton is transferred to an amine nitrogen atom, eventually causing complex dissociation [89]. On the contrary, protonation of pyridine or thiazol pendants requires decoordination of the pendant arm [61].

3.3. Cyclic voltammetry

Cyclic voltammetry measurements were carried out to analyse the redox stability of the $[Cu(CB-TE1A)]^+$, $[Cu(NO2Th)]^{2+}$ and $[Cu(NO2Py)]^{2+}$ complexes. Electrochemical experiments were recorded using solutions of the complexes in 0.15 M NaCl and a Ag/AgCl
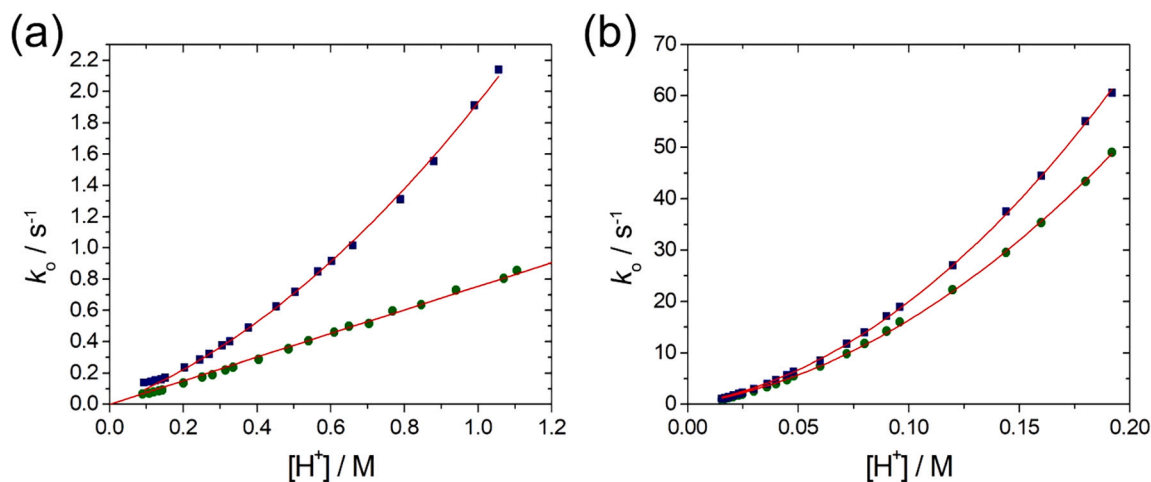

Fig. 4. Variation of k_o with proton concentration for $[Cu(NO2A)]$ (a) and $[Cu(tO2DO2A)]$ (b) using $NaClO_4$ (●) or NaCl (■) to adjust the ionic strength ($I = 1$ M and 0.5 M for $[Cu(NO2A)]$ and $[Cu(tO2DO2A)]$, respectively).

reference electrode. Both [Cu(CB-TE1A)]$^+$ and [Cu(NO2Py)]$^{2+}$ are characterized by reversible voltammograms with $E^\circ = -0.92$ V ($\Delta E_p =$ 80 mV) and $E^\circ = -0.61$ V ($\Delta E_p =$ 80 mV), respectively (*vs* Ag/AgCl, Fig. 5). These redox potentials correspond to $E^\circ = -0.71$ V and $E^\circ = -0.40$ V with respect to the NHE [96]. The reduction potential of [Cu (CB-TE1A)]$^+$ is therefore clearly out of the threshold for common bio-reductants (-0.4 V *vs* NHE), while the reduction potential of [Cu (NO2Py)]$^{2+}$ is right in the edge. The anodic and cathodic peak currents show linear dependence with the square root of the scan rate (Fig. S23 and S24, Supporting Information), which points to diffusion controlled electrochemical processes [97].

The cyclic voltammogram of the [Cu(NO2Th)]$^{2+}$ complex is somewhat more complicated. It shows a reversible system with $E^\circ = -0.46$ V ($\Delta E_p =$ 80 mV) *vs* Ag/AgCl, which corresponds to -0.25 *vs* NHE. A very similar potential was observed previously using 0.1 M LiClO$_4$ as the electrolyte (-0.47 V) [60]. However, a new peak is also observed at $E \sim$ -0.26 V that is more prominent when using low scan rates (Fig. S16, Supporting Information). This suggests that the reduced Cu(I) species experiences some rearrangement within the scale of the cyclic voltammetry experiment. This behavior was not observed previously in 0.1 M LiClO$_4$, suggesting that chloride coordination may be involved in the rearrangement of the Cu(I) coordination environment. The stability constant of the Cu(I) complex of NO2Th can be estimated from the electrochemical data and the stability constant of the Cu(II) complex (log $K_{Cu(II)} = 20.77$), using the methodology reported previously [98,99]. Taking a standard electrode potential for the Cu$_{aq}^{2+}$/Cu$_{aq}^+$ redox potential of 0.13 V [98], we obtain log $K_{Cu(I)} = 14.4$. This stability constant is similar to those reported for the Cu(I) complexes with polydentate ligands containing S donor atoms [100].

The cyclic voltammograms of the [Cu(NO2A)] and [Cu(tO2DO2A)] complexes are characterized by irreversible reduction waves at -0.86 and -0.48 V *vs.* Ag/AgCl, respectively, with additional features being observed in the back scans (Fig. S25). This indicates an important reorganization of the metal coordination sphere upon reduction to Cu(I). An oxidative stripping peak of Cu(0) to Cu (II) is also observed at around 0.0 V [101], indicating dissociation of the Cu(I) complex.

3.4. Dissociation in the presence of ascorbate

The reactivity of the [Cu(CB-TE1A)]$^+$, [Cu(NO2Th)]$^{2+}$ and [Cu (NO2Py)]$^{2+}$ complexes in the presence of ascorbate (oxo-3-gulofuranolactone acid, better known as vitamin C) was investigated using spectrophotometric measurements. Ascorbate is a common bioreducing agent with a number of important biological functions [102]. It readily
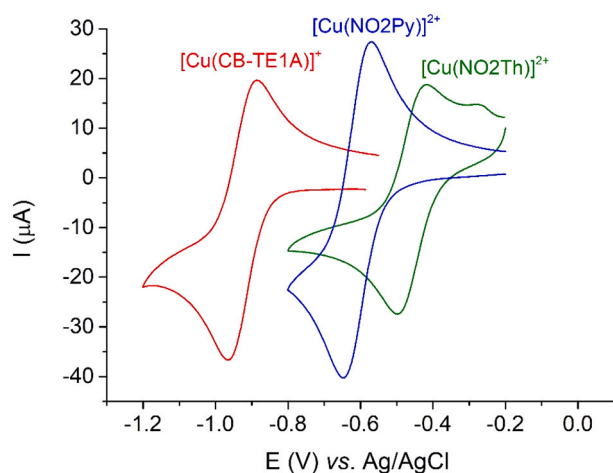
Fig. 5. Cyclic voltammograms recorded from aqueous solutions of [Cu(CB-TE1A)]$^+$ (1.8 mM, pH = 6.6), [Cu(NO2Th)]$^{2+}$ (1.7 mM, pH = 6.3) and [Cu (NO2Py)]$^{2+}$ (1.9 mM, pH = 8.4).

experiences two consecutive one-electron oxidations to form dehydroascorbic acid [103,104]. Kinetic experiments were conducted using neocuproine (NC, 2,9-dimethyl-1,10-phenanthroline) as a Cu(I) scavenger, as it forms a stable complex with Cu(I) (log $\beta_2 = 19.1$) characterized by a strong absorption at 450 nm [105,106]. Experiments were performed using phosphate buffer to keep the pH at 7.1 and ionic strength lower than 0.2 M, unless when analysing the effect of pH and ionic strength. No reactivity was observed for the [Cu(CB-TE1A)]$^+$ and [Cu(NO2Py)]$^{2+}$ complexes, as would be expected given the rather negative reduction potentials evidenced by cyclic voltammetry experiments. The [Cu(NO2Th)]$^{2+}$ complex is reduced by both ascorbate and glutathione, which are probably the most important reducing agents in living tissues [107]. However, reduction in the presence of glutathione was found to be fast, but the absorption spectra experienced further changes with time once the reaction was complete (Fig. S26, Supporting Information). Thus, further experiments were carried out in the presence of ascorbate.

Addition of [Cu(NO2Th)]$^{2+}$ (51.8 μM) to a solution of ascorbate (8.67 mM) and NC provokes a slow increase with time of the absorbance of the [Cu(NC)$_2$]$^+$ complex at 454 nm (Fig. 6). The kinetic traces are characteristic of a pseudo-first-order process if [NC]/[CuNO2Th^{2+}] > 2. The Cu(II) complex was the last reagent added to the mixture, as otherwise complex kinetic traces are observed. The observed rate constants remain identical within experimental error regardless the concentration of [Cu(NO2Th)]$^{2+}$ with a value of $k_0 = 4.7 \pm 0.1 \times 10^{-4}$ s^{-1}. The values of A_∞ show a linear dependence with the concentration of the complex with negligible intercept and a slope of 6280 mol^{-1}dm^{3}cm^{-1}. The rate constants are not affected by the concentration of phosphate buffer in the 0.05–0.32 M concentration range, nor by the concentration of NC (0.087–0.291 mM), providing that [NC]/[CuNO2Th^{2+}] > 2 (See Tables S1-S2, Supporting Information).

Experiments performed with constant concentrations of [Cu (NO2Th)]$^{2+}$ (52.5 μM) and NC (0.148 M) at pH 7.1 evidence a linear dependence with the concentration of ascorbate (Fig. 6) according to:

$$k_o = k_1 + k_2[\text{Ascorbate}] \tag{14}$$

The linear fit of the data afforded $k_1 = 7.0 \pm 0.6 \times 10^{-5}$ s^{-1} and $k_2 = 5.27 \pm 0.06 \times 10^{-2}$ M^{-1} s^{-1}. The non-negligible y-intercept suggests a reversible process, likely due to the formation of a ternary complex between ascorbate and the complex. Indeed, previous studies showed that the slow (rate-determining) step for the oxidation of ascorbate by Cu(II) complexes is the formation of a ternary complex with ascorbate [108,109]. For [Cu(NO2Th)]$^{2+}$, this is supported by the plot of A_∞-A_0 *versus* ascorbate concentration, which shows a saturation profile (Fig. S27, Supporting Information). Thus, k_2 and k_1 can be related to the rate constants characterizing the forward and reverse reactions responsible for the formation and dissociation of the ternary complex between [Cu(NO2Th)]$^{2+}$ and ascorbate. The association constant can therefore be estimated as $K = k_2/k_1 = 753 \pm 73$ M^{-1}.

The rate constants are significantly affected by the ionic strength of the medium adjusted with NaCl, as predicted by the Brønsted-Bjerrum Equation [110]:

$$logk = logk_0 + 2A_D z_A z_B \frac{\sqrt{I}}{1 + \sqrt{I}}. \tag{15}$$

In this expression, k_0 is the rate constant extrapolated to infinite dilution, I is the ionic strength of the medium and A_D is a constant that permits the calculation of activity coefficients with the Debye-Hückel eq. A plot of log k *versus* $\sqrt{I}/(1 + \sqrt{I})$ is linear with a negative slope of -2.15 ± 0.07 and an intercept that corresponds to $k_0 = 1.78 \times 10^{-3}$ s^{-1} (Fig. 7). The slope of the plot is in good agreement with that expected for the reaction of the [Cu(NO2Th)]$^{2+}$ complex and monohydrogen ascorbate, which is largely predominating at neutral pH [111], taking into account the theoretical value of A_D at 25 °C (0.51) [112].

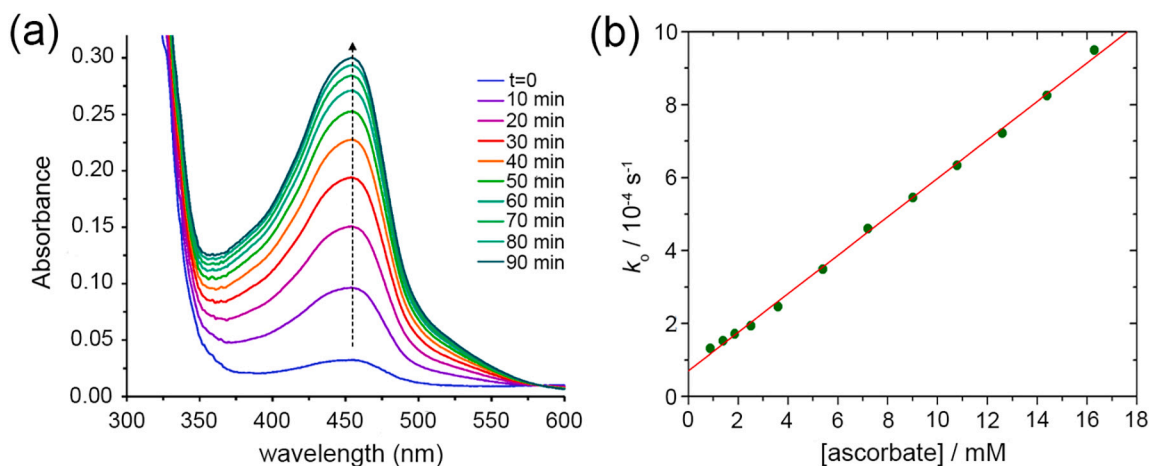The rate constants vary significantly with the pH of the medium,

Fig. 6. (a) Spectral changes observed with time for $[Cu(NO2Th)]^{2+}$ (51.8 μM) in the presence of NC (0.233 mM) and ascorbate (8.67 mM) in $HPO_4^{2-}/H_2PO_4^-$ buffer (0.083 M, pH 7.2, $I = 0.15$). (b) Variation of k_o with ascorbate concentration at pH 7.1 ($[Cu(NO2Th)]^{2+}$ concentration, 52.5 μM; [NC] = 0,148 M; pH 7.1).
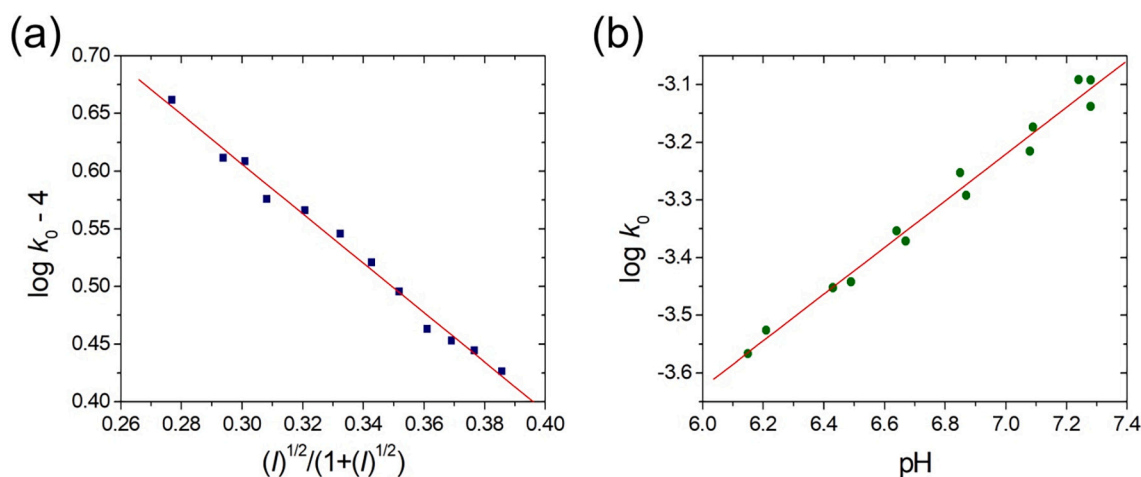

Fig. 7. (a) Effect of ionic strength adjusted with NaCl on the dissociation of $[Cu(NO2Th)]^{2+}$ (46.9 μM) in the presence of NC (0.132 mM) and ascorbate (5.4 mM) in $HPO_4^{2-}/H_2PO_4^-$ buffer (0.083 M, pH 7.2). (b) Variation of $\log k_o$ with pH ($[Cu(NO2Th)]^{2+}$ concentration, 52.5 μM; [NC] = 0,148 M; ascorbate 8.66 mM, $HPO_4^{2-}/H_2PO_4^-$ 0.15 M).

which was varied in the range (6.05 < pH < 7.28) using $HPO_4^{2-}/H_2PO_4^-$ buffer, maintaining approximately constant ionic strengths (0.20–0.26 M). These experiments evidence a significant increase of the rate constants with pH (Fig. 7). A plot of $\log k_0$ *versus* pH evidences a linear dependence with a slope of 0.40 ± 0.2, which points to a complicated dependence of the rate constants with pH.

The half-life of the $[Cu(NO2Th)]^{2+}$ complex under physiological conditions can be estimated with Eq. (12) by considering a concentration of the ascorbate anion *in vivo* of 43 μM [113], affording $\tau_{1/2} = \ln 2/k_o = 2.7$ h. Thus, this complex is expected to display a rather fast dissociation under physiological conditions upon reduction by ascorbate, in spite of the very high inertness following the acid-catalyzed mechanism. A similar behavior was observed recently for Fe(III) complexes proposed as contrast agents for magnetic resonance imaging [114]. Thus, a critical issue that must be considered when designing both Cu(II) or Fe(III) complexes for biomedical applications is to shift the reduction potential below the window accessible by bioreductants.

4. Conclusions

In this work we have investigated different dissociation pathways that may result in the dissociation of Cu(II) complexes *in vivo*. This is a

very relevant issue to develop radiopharmaceuticals based on Cu radioisotopes. Our studies revealed that the nature of the counterion present in solution (perchlorate or chloride) may have a significant influence in the dissociation of the complexes following the acid-assisted pathway. This is an issue that must be considered when testing the inertness of Cu(II) complexes, given the high concentrations of the chloride anion *in vivo*. Chloride coordination likely facilitates the protonation of ligand donor atoms, such as carboxylate donors, triggering complex dissociation by a cascade of events in which the proton is transferred to an amine N atom of the macrocycle. Anion coordination reduces the positive charge of the complex, and this makes complex protonation more likely to occur. Studies investigating the kinetics of decomplexation of Cu(II) complexes using different electrolytes are rare, and the results reported here show that this is an issue that should be carefully considered. An accelerating effect in complex dissociation caused by chloride addition was described before for a few Cu(II) complexes [27,115]. The potential effect of other anions present *in vivo* (i. e. carbonate, phosphate, citrate or lactate) is yet to be deciphered. A comparison of the dissociation kinetics of [Cu(NO2A)] and [Cu(tO2DO2A)] suggests that the ability of chloride to accelerate complex dissociation is more likely to occur in five-coordinate complexes (i. e. [Cu(NO2A)]) than in six-coordinate complexes like [Cu(tO2DO2A)]. On

the contrary, five-coordinate complexes were found to be more inert than six-coordinate analogues due to the Jahn-Teller effect operating in the latter.

The charge of the complex is also important, as positively charged complexes are likely more inert with respect to their dissociation following the acid-catalyzed mechanism. This becomes clear by comparing the inertness of $[Cu(NO2Th)]^{2+}$, $[Cu(NO2Py)]^{2+}$ and $[Cu(NO2A)]$, which are all based on pentadentate ligands derived from the same triazacyclononane platform. The neutral $[Cu(NO2A)]$ complex experiences relatively fast dissociation following the acid-catalyzed mechanism, while the structurally-related positively charged analogues are extremely inert under acidic conditions.

One of the main findings of this study is the fast dissociation of $[Cu(NO2Th)]^{2+}$ in the presence of ascorbic acid, which is a typical bioreductant. This is in sharp contrast to the astonishing inertness of this complex observed under acidic conditions. Conversely, the $[Cu(NO2Py)]^{2+}$ and $[Cu(CB-TE1A)]^{+}$ complexes do not dissociate in the presence of ascorbate, as their reduction potentials are more negative than that of $[Cu(NO2Th)]^{2+}$, as revealed by cyclic voltammetry experiments. Thus, this work highlights the importance of shifting the reduction potentials of Cu(II) complexes for PET applications out of the window of bioreducing agents.

Funding

Author statement

David Esteban-Gómez and Carlos Platas-Iglesias conceived and designed the experiments; Rocío Uzal-Varela synthetized and isolated the complexes; Raphaël Tripier and Veronique Patinec contributed to the synthesis of the ligands and complexes; Emilia Iglesias performed the kinetic experiments and analysed the kinetic data; Moisés Canle and Carlos Platas-Iglesias participated in analysing the data; Marcelino Maneiro and Rocío Uzal-Varela performed the cyclic voltammetry experiments, Laura Valencia performed the X-ray crystal structure determination; David Esteban-Gómez and Emilia Iglesias supervised the research and prepared the article. All authors participated in the preparation of the manuscript.

Declaration of Competing Interest

The authors declare no conflict of interest.

Data availability

Data will be made available on request.

Appendix A. Supplementary data

Supplementary data to this article can be found online at https://doi.org/10.1016/j.jinorgbio.2022.111951.

References

[1] S.M. Ametamey, M. Honer, P.A. Schubiger, Molecular imaging with PET, Chem. Rev. 108 (2008) 1501–1516, https://doi.org/10.1021/cr0782426.

[2] S.S. Gambhir, Molecular imaging of cancer with positron emission tomography, Nat. Rev. Cancer 2 (2002) 683–693, https://doi.org/10.1038/nrc882.

[3] V. Pichler, N. Berroterán-Infante, C. Philippe, C. Vraka, E.-M. Klebermass, T. Balber, S. Pfaff, L. Nics, M. Mitterhauser, W. Wadsak, An overview of PET radiochemistry, part 1: the covalent labels ^{18}F, ^{11}C, and ^{13}N, J. Nucl. Med. 59 (2018) 1350–1354, https://doi.org/10.2967/jnumed.117.190793.

[4] E. Boros, A.B. Packard, Radioactive transition metals for imaging and therapy, Chem. Rev. 119 (2019) 870–901, https://doi.org/10.1021/acs.chemrev.8b00281.

[5] T.I. Kostelnik, C. Orvig, Radioactive Main group and rare earth metals for imaging and therapy, Chem. Rev. 119 (2019) 902–956, https://doi.org/10.1021/acs.chemrev.8b00294.

[6] C.J. Anderson, R. Ferdani, Copper-64 radiopharmaceuticals for PET imaging of Cancer: advances in preclinical and clinical research, Cancer Biother. Radiopharm. 24 (2009) 379–393, https://doi.org/10.1089/cbr.2009.0674.

[7] Y. Zhou, J. Li, X. Xu, M. Zhao, B. Zhang, S. Deng, Y. Wu, ^{64}Cu-based radiopharmaceuticals in molecular imaging, Technol. Cancer Res. Treat. 18 (2019), https://doi.org/10.1177/1533033819830758, 153303381983075.

[8] P. Adumeau, S.K. Sharma, C. Brent, B.M. Zeglis, Site-specifically labeled Immunoconjugates for molecular imaging—part 2: peptide tags and unnatural amino acids, Mol. Imaging Biol. 18 (2016) 153–165, https://doi.org/10.1007/s11307-015-0920-y.

[9] P. Adumeau, S.K. Sharma, C. Brent, B.M. Zeglis, Site-specifically labeled Immunoconjugates for molecular imaging—part 1: cysteine residues and Glycans, Mol. Imaging Biol. 18 (2016) 1–17, https://doi.org/10.1007/s11307-015-0919-4.

[10] C.F. Ramogida, C. Orvig, Tumour targeting with radiometals for diagnosis and therapy, Chem. Commun. 49 (2013) 4720, https://doi.org/10.1039/c3cc41554f.

[11] M.D. Bartholomä, Recent developments in the design of bifunctional chelators for metal-based radiopharmaceuticals used in positron emission tomography, Inorganica Chim. Acta. 389 (2012) 36–51, https://doi.org/10.1016/j.ica.2012.01.061.

[12] E.W. Price, C. Orvig, Matching chelators to radiometals for radiopharmaceuticals, Chem. Soc. Rev. 43 (2014) 260–290, https://doi.org/10.1039/C3CS60304K.

[13] T.W. Price, J. Greenman, G.J. Stasiuk, Current advances in ligand design for inorganic positron emission tomography tracers ^{68}Ga, ^{64}Cu, ^{89}Zr and ^{44}Sc, Dalton Trans. 45 (2016) 15702–15724, https://doi.org/10.1039/C5DT04706D.

[14] Z. Cai, C.J. Anderson, Chelators for copper radionuclides in positron emission tomography radiopharmaceuticals: chelators for copper radionuclides in PET radiopharmaceuticals, J. Label. Compd. Radiopharm. 57 (2014) 224–230, https://doi.org/10.1002/jlcr.3165.

[15] R. Chakravarty, S. Chakraborty, A. Dash, $^{64}Cu^{2+}$ ions as PET probe: An emerging paradigm in molecular imaging of Cancer, Mol. Pharm. 13 (2016) 3601–3612, https://doi.org/10.1021/acs.molpharmaceut.6b00582.

[16] C. Qin, H. Liu, K. Chen, X. Hu, X. Ma, X. Lan, Y. Zhang, Z. Cheng, Theranostics of malignant melanoma with $^{64}CuCl_2$, J. Nucl. Med. 55 (2014) 812–817, https://doi.org/10.2967/jnumed.113.133850.

[17] S.N. Rylova, C. Stoykow, L. Del Pozzo, K. Abiraj, M.L. Tamma, Y. Kiefer, M. Fani, H.R. Maecke, The somatostatin receptor 2 antagonist 64Cu-NODAGA-JR11 outperforms ^{64}Cu-DOTA-TATE in a mouse xenograft model, PLoS One 13 (2018), e0195802, https://doi.org/10.1371/journal.pone.0195802.

[18] L.A. Bass, M. Wang, M.J. Welch, C.J. Anderson, In vivo Transchelation of Copper-64 from TETA-octreotide to superoxide dismutase in rat liver, Bioconjug. Chem. 11 (2000) 527–532, https://doi.org/10.1021/bc990167l.

[19] C.B. Johnbeck, U. Knigge, A. Loft, A.K. Berthelsen, J. Mortensen, P. Oturai, S. W. Langer, D.R. Elema, A. Kjaer, Head-to-head comparison of ^{64}Cu-DOTATATE and ^{68}Ga-DOTATOC PET/CT: a prospective study of 59 patients with neuroendocrine tumors, J. Nucl. Med. 58 (2017) 451–457, https://doi.org/10.2967/jnumed.116.180430.

[20] G.J. Stasiuk, N.J. Long, The ubiquitous DOTA and its derivatives: the impact of 1,4,7,10-tetraazacyclododecane-1,4,7,10-tetraacetic acid on biomedical imaging, Chem. Commun. 49 (2013) 2732, https://doi.org/10.1039/c3cc38507h.

[21] Y. Zhang, H. Hong, J.W. Engle, J. Bean, Y. Yang, B.R. Leigh, T.E. Barnhart, W. Cai, Positron emission tomography imaging of CD105 expression with a ^{64}Cu-labeled monoclonal antibody: NOTA is superior to DOTA, PLoS One 6 (2011), e28005, https://doi.org/10.1371/journal.pone.0028005.

[22] M.R. Lewis, C.A. Boswell, R. Laforest, T.L. Buettner, D. Ye, J.M. Connett, C. J. Anderson, Conjugation of monoclonal antibodies with TETA using activated esters: biological comparison of ^{64}Cu-TETA-1A3 with ^{64}Cu-BAT-2IT-1A3, Cancer Biother. Radiopharm. 16 (2001) 483–494, https://doi.org/10.1089/10849780152752083.

[23] T. Le Bihan, C.H.S. Driver, T. Ebenhan, N. Le Bris, J.R. Zeevaart, R. Tripier, *In vivo* albumin-binding of a *C*-functionalized Cyclam platform for ^{64}Cu-PET/CT imaging in breast Cancer model, ChemMedChem. 16 (2021) 809–821, https://doi.org/10.1002/cmdc.202000800.

[24] Z. Halime, M. Frindel, N. Camus, P.-Y. Orain, M. Lacombe, M. Chérel, J.-F. Gestin, A. Faivre-Chauvet, R. Tripier, New synthesis of phenyl-isothiocyanate C-functionalised cyclams. Bioconjugation and ^{64}Cu phenotypic PET imaging studies of multiple myeloma with the TE2A derivative, Org. Biomol. Chem. 13 (2015) 11302–11314, https://doi.org/10.1039/C5OB01618E.

[25] D.N. Pandya, J.Y. Kim, J.C. Park, H. Lee, P.B. Phapale, W. Kwak, T.H. Choi, G. J. Cheon, Y.-R. Yoon, J. Yoo, Revival of TE2A; a better chelate for cu(II) ions than TETA? Chem. Commun. 46 (2010) 3517–3519, https://doi.org/10.1039/b925703a.

[26] A.V. Dale, D.N. Pandya, J.Y. Kim, H. Lee, Y.S. Ha, N. Bhatt, J. Kim, J.J. Seo, W. Lee, S.H. Kim, Y.-R. Yoon, G.I. An, J. Yoo, Non-cross-bridged Tetraazamacrocyclic Chelator for stable ^{64}Cu-based radiopharmaceuticals, ACS Med. Chem. Lett. 4 (2013) 927–931, https://doi.org/10.1021/ml400142s.

[27] J. Kotek, P. Lubal, P. Hermann, I. Císařová, I. Lukeš, T. Godula, I. Svobodová, P. Táborský, J. Havel, High thermodynamic stability and extraordinary kinetic inertness of copper(II) complexes with 1,4,8,11-Tetraazacyclotetradecane-1,8-bis (methylphosphonic acid): example of a rare isomerism between kinetically inert Penta- and Hexacoordinated copper(II) complexes, Chem. Eur. J. 9 (2003) 233–248, https://doi.org/10.1002/chem.200390017.

[28] I. Svobodová, J. Havlíčková, J. Plutnar, P. Lubal, J. Kotek, P. Hermann, Metal complexes of 4,11-Dimethyl-1,4,8,11-tetraazacyclotetradecane-1,8-bis(methyl-phosphonic acid) - thermodynamic and formation/Decomplexation kinetic studies, Eur. J. Inorg. Chem. 2009 (2009) 3577–3592, https://doi.org/10.1002/ejic.200900358.

[29] T. David, V. Hlinová, V. Kubíček, R. Bergmann, F. Striese, N. Berndt, D. Szöllősi, T. Kovács, D. Máthé, M. Bachmann, H.-J. Pietzsch, P. Hermann, Improved conjugation, 64-cu radiolabeling, in vivo stability, and imaging using nonprotected bifunctional macrocyclic ligands: Bis(Phosphinate) Cyclam (BPC) chelators, J. Med. Chem. 61 (2018) 8774–8796, https://doi.org/10.1021/acs.jmedchem.8b00932.

[30] M. Frindel, N. Camus, A. Rauscher, M. Bourgeois, C. Alliot, L. Barré, J.-F. Gestin, R. Tripier, A. Faivre-Chauvet, Radiolabeling of HTE1PA: a new monopicolinate cyclam derivative for cu-64 phenotypic imaging. In vitro and in vivo stability studies in mice, Nucl. Med. Biol. 41 (2014) e49–e57, https://doi.org/10.1016/j.nucmedbio.2013.12.009.

[31] M. Frindel, P. Le Saëc, M. Beyler, A.-S. Navarro, C. Saï-Maurel, C. Alliot, M. Chérel, J.-F. Gestin, A. Faivre-Chauvet, R. Tripier, Cyclam te1pa for 64Cu PET imaging. Bioconjugation to antibody, radiolabeling and preclinical application in xenografted colorectal cancer, RSC Adv. 7 (2017) 9272–9283, https://doi.org/10.1039/C6RA26003A.

[32] T. Le Bihan, A.-S. Navarro, N. Le Bris, P. Le Saëc, S. Gouard, F. Haddad, J.-F. Gestin, M. Chérel, A. Faivre-Chauvet, R. Tripier, Synthesis of C -functionalized TE1PA and comparison with its analogues. An example of bioconjugation on 9E7.4 mAb for 64Cu-PET imaging, Org. Biomol. Chem. 16 (2018) 4261–4271, https://doi.org/10.1039/C8OB00499D.

[33] A.-S. Navarro, T. Le Bihan, P. Le Saëc, N.L. Bris, C. Bailly, C. Saï-Maurel, M. Bourgeois, M. Chérel, R. Tripier, A. Faivre-Chauvet, TE1PA as innovating Chelator for 64Cu Immuno-TEP imaging: a comparative in vivo study with DOTA/NOTA by conjugation on 9E7.4 mAb in a syngeneic multiple myeloma model, Bioconjug. Chem. 30 (2019) 2393–2403, https://doi.org/10.1021/acs.bioconjchem.9b00510.

[34] R.A. Dumont, F. Deininger, R. Haubner, H.R. Maecke, W.A. Weber, M. Fani, Novel 64Cu- and 68Ga-labeled RGD conjugates show improved PET imaging of $\alpha_v\beta_3$ integrin expression and facile Radiosynthesis, J. Nucl. Med. 52 (2011) 1276–1284, https://doi.org/10.2967/jnumed.111.087700.

[35] D.N. Pandya, A.V. Dale, J.Y. Kim, H. Lee, Y.S. Ha, G.I. An, J. Yoo, New macrobicyclic Chelator for the development of Ultrastable 64Cu-radiolabeled bioconjugate, Bioconjug. Chem. 23 (2012) 330–335, https://doi.org/10.1021/bc200539t.

[36] C.A. Boswell, X. Sun, W. Niu, G.R. Weisman, E.H. Wong, A.L. Rheingold, C.J. Anderson, Comparative in vivo stability of Copper-64-labeled cross-bridged and conventional Tetraazamacrocyclic complexes, J. Med. Chem. 47 (2004) 1465–1474, https://doi.org/10.1021/jm030383m.

[37] J.E. Sprague, Y. Peng, A.L. Fiamengo, K.S. Woodin, E.A. Southwick, G.R. Weisman, E.H. Wong, J.A. Golen, A.L. Rheingold, C.J. Anderson, Synthesis, characterization and in vivo studies of cu(II)-64-labeled cross-bridged Tetraazamacrocycle-amide complexes as models of peptide conjugate imaging agents, J. Med. Chem. 50 (2007) 2527–2535, https://doi.org/10.1021/jm070204r.

[38] W. Liu, G. Hao, M.A. Long, T. Anthony, J.-T. Hsieh, X. Sun, Imparting Multivalency to a bifunctional Chelator: a scaffold Design for Targeted PET imaging probes, Angew. Chem. Int. Ed. 48 (2009) 7346–7349, https://doi.org/10.1002/anie.200903556.

[39] C.A. Boswell, C.A.S. Regino, K.E. Baidoo, K.J. Wong, A. Bumb, H. Xu, D.E. Milenic, J.A. Kelley, C.C. Lai, M.W. Brechbiel, Synthesis of a cross-bridged Cyclam derivative for peptide conjugation and 64Cu radiolabeling, Bioconjug. Chem. 19 (2008) 1476–1484, https://doi.org/10.1021/bc800039w.

[40] X. Sun, M. Wuest, G.R. Weisman, E.H. Wong, D.P. Reed, C.A. Boswell, R. Motekaitis, A.E. Martell, M.J. Welch, C.J. Anderson, Radiolabeling and in vivo behavior of Copper-64-labeled cross-bridged Cyclam ligands, J. Med. Chem. 45 (2002) 469–477, https://doi.org/10.1021/jm0103817.

[41] R. Ferdani, D.J. Stigers, A.L. Fiamengo, L. Wei, B.T.Y. Li, J.A. Golen, A.L. Rheingold, G.R. Weisman, E.H. Wong, C.J. Anderson, Synthesis, cu(II) complexation, 64Cu-labeling and biological evaluation of cross-bridged cyclam chelators with phosphonate pendant arms, Dalton Trans. 41 (2012) 1938–1950, https://doi.org/10.1039/C1DT11743B.

[42] L.M.P. Lima, Z. Halime, R. Marion, N. Camus, R. Delgado, C. Platas-Iglesias, R. Tripier, Monopicolinate cross-bridged Cyclam combining very fast complexation with very high stability and inertness of its copper(II) complex, Inorg. Chem. 53 (2014) 5269–5279, https://doi.org/10.1021/ic500491c.

[43] R.C. Knighton, T. Troadec, V. Mazan, P. Le Saëc, S. Marionneau-Lambot, T. Le Bihan, N. Saffon-Merceron, N. Le Bris, M. Chérel, A. Faivre-Chauvet, M. Elhabiri, L.J. Charbonnière, R. Tripier, Cyclam-based chelators bearing Phosphonated pyridine pendants for 64Cu-PET imaging: synthesis, physicochemical studies, radiolabeling, and bioimaging, Inorg. Chem. 60 (2021) 2634–2648, https://doi.org/10.1021/acs.inorgchem.0c03492.

[44] S. Litau, U. Seibold, A. Vall-Sagarra, G. Fricker, B. Wängler, C. Wängler, Comparative assessment of complex stabilities of Radiocopper chelating agents by a combination of complex challenge and in vivo experiments, ChemMedChem. 10 (2015) 1200–1208, https://doi.org/10.1002/cmdc.201500132.

[45] P. Comba, M. Kubeil, J. Pietzsch, H. Rudolf, H. Stephan, K. Zarschler, Bispidine Dioxotetraaza macrocycles: a new class of Bispidines for 64Cu PET imaging, Inorg. Chem. 53 (2014) 6698–6707, https://doi.org/10.1021/ic500476u.

[46] S. Juran, M. Walther, H. Stephan, R. Bergmann, J. Steinbach, W. Kraus, F. Emmerling, P. Comba, Hexadentate Bispidine derivatives as versatile bifunctional chelate agents for copper(II) radioisotopes, Bioconjug. Chem. 20 (2009) 347–359, https://doi.org/10.1021/bc800461e.

[47] A. Roux, A.M. Nonat, J. Brandel, V. Hubscher-Bruder, L.J. Charbonnière, Kinetically inert Bispidol-based cu(II) chelate for potential application to 64/67Cu nuclear medicine and diagnosis, Inorg. Chem. 54 (2015) 4431–4444, https://doi.org/10.1021/acs.inorgchem.5b00207.

[48] M.S. Cooper, M.T. Ma, K. Sunassee, K.P. Shaw, J.D. Williams, R.L. Paul, P.S. Donnelly, P.J. Blower, Comparison of 64Cu-complexing bifunctional chelators for Radioimmunoconjugation: labeling efficiency, specific activity, and in vitro / in vivo stability, Bioconjug. Chem. 23 (2012) 1029–1039, https://doi.org/10.1021/bc300037w.

[49] N. Di Bartolo, A.M. Sargeson, S.V. Smith, New 64Cu PET imaging agents for personalised medicine and drug development using the hexa-aza cage, SarAr, Org. Biomol. Chem. 4 (2006) 3350, https://doi.org/10.1039/b605615f.

[50] M. Shokeen, C.J. Anderson, Molecular imaging of Cancer with Copper-64 radiopharmaceuticals and positron emission tomography (PET), Acc. Chem. Res. 42 (2009) 832–841, https://doi.org/10.1021/ar800255q.

[51] T.M. Jones-Wilson, K.A. Deal, C.J. Anderson, D.W. McCarthy, Z. Kovacs, R.J. Motekaitis, A.D. Sherry, A.E. Martell, M.J. Welch, The in vivo behavior of copper-64-labeled azamacrocyclic complexes, Nucl. Med. Biol. 25 (1998) 523–530, https://doi.org/10.1016/S0969-8051(98)00017-1.

[52] M. Persson, M. Hosseini, J. Madsen, T.J.D. Jørgensen, K.J. Jensen, A. Kjaer, M. Ploug, Improved PET imaging of uPAR expression using new 64Cu-labeled cross-bridged peptide ligands: comparative in vitro and in vivo studies, Theranostics. 3 (2013) 618–632, https://doi.org/10.7150/thno.6810.

[53] K.S. Woodin, K.J. Heroux, C.A. Boswell, E.H. Wong, G.R. Weisman, W. Niu, S.A. Tomellini, C.J. Anderson, L.N. Zakharov, A.L. Rheingold, Kinetic inertness and electrochemical behavior of copper(II) Tetraazamacrocyclic complexes: possible implications for in vivo stability, Eur. J. Inorg. Chem. 2005 (2005) 4829–4833, https://doi.org/10.1002/ejic.200500579.

[54] T.J. Wadas, E.H. Wong, G.R. Weisman, C.J. Anderson, Coordinating Radiometals of copper, gallium, indium, yttrium, and zirconium for PET and SPECT imaging of disease, Chem. Rev. 110 (2010) 2858–2902, https://doi.org/10.1021/cr900325h.

[55] E. Boros, J.F. Cawthray, C.L. Ferreira, B.O. Patrick, M.J. Adam, C. Orvig, Evaluation of the H2dedpa scaffold and its cRGDyK conjugates for labeling with 64Cu, Inorg. Chem. 51 (2012) 6279–6284, https://doi.org/10.1021/ic300482x.

[56] A. Guillou, L.M.P. Lima, D. Esteban-Gómez, R. Delgado, C. Platas-Iglesias, V. Patinec, R. Tripier, Endo - versus exo -cyclic coordination in copper complexes with methylthiazolylcarboxylate tacn derivatives, Dalton Trans. 48 (2019) 8740–8755, https://doi.org/10.1039/C9DT01366K.

[57] F. Baark, F. Shaughnessy, V.R. Pell, J.E. Clark, T.R. Eykyn, P. Blower, R. Southworth, Tissue acidosis does not mediate the hypoxia selectivity of [64Cu][cu(ATSM)] in the isolated perfused rat heart, Sci. Rep. 9 (2019) 499, https://doi.org/10.1038/s41598-018-36145-1.

[58] M.G. Handley, R.A. Medina, E. Nagel, P.J. Blower, R. Southworth, PET imaging of cardiac hypoxia: opportunities and challenges, J. Mol. Cell. Cardiol. 51 (2011) 640–650, https://doi.org/10.1016/j.yjmcc.2011.07.005.

[59] J.L. Dearling, J.S. Lewis, G.E. Mullen, M.J. Welch, P.J. Blower, Copper bis (thiosemicarbazone) complexes as hypoxia imaging agents: structure-activity relationships, JBIC J. Biol. Inorg. Chem. 7 (2002) 249–259, https://doi.org/10.1007/s007750100291.

[60] M. Le Fur, M. Beyler, N. Le Poul, L.M.P. Lima, Y. Le Mest, R. Delgado, C. Platas-Iglesias, V. Patinec, R. Tripier, Improving the stability and inertness of cu(II) and cu(I) complexes with methylthiazolyl ligands by tuning the macrocyclic structure, Dalton Trans. 45 (2016) 7406–7420, https://doi.org/10.1039/C6DT00385K.

[61] A. Guillou, L.M.P. Lima, D. Esteban-Gómez, N. Le Poul, M.D. Bartholomä, C. Platas-Iglesias, R. Delgado, V. Patinec, R. Tripier, Methylthiazolyl Tacn ligands for copper complexation and their bifunctional chelating agent derivatives for bioconjugation and Copper-64 radiolabeling: An example with Bombesin, Inorg. Chem. 58 (2019) 2669–2685, https://doi.org/10.1021/acs.inorgchem.8b03280.

[62] S.J. Brudenell, L. Spiccia, E.R.T. Tiekink, Binuclear copper(II) complexes of Bis (pentadentate) ligands derived from alkyl-bridged Bis(1,4,7-triazacyclonane) macrocycles, Inorg. Chem. 35 (1996) 1974–1979, https://doi.org/10.1021/ic951146f.

[63] F.K. Kálmán, V. Nagy, R. Uzal-Varela, P. Pérez-Lourido, D. Esteban-Gómez, Z. Garda, K. Pota, R. Mezei, A. Pallier, É. Tóth, C. Platas-Iglesias, G. Tircsó, Expanding the ligand classes used for Mn(II) complexation: Oxa-aza macrocycles make the difference, Molecules. 26 (2021) 1524, https://doi.org/10.3390/molecules26061524.

[64] G.A. McLachlan, G.D. Fallon, R.L. Martin, L. Spiccia, Synthesis, structure and properties of five-coordinate copper(II) complexes of Pentadentate ligands with Pyridyl pendant arms, Inorg. Chem. 34 (1995) 254–261, https://doi.org/10.1021/ic00105a041.

[65] M. Roger, L.M.P. Lima, M. Frindel, C. Platas-Iglesias, J.-F. Gestin, R. Delgado, V. Patinec, R. Tripier, Monopicolinate-dipicolyl derivative of Triazacyclononane for stable complexation of Cu^{2+} and 64Cu^{2+}, Inorg. Chem. 52 (2013) 5246–5259, https://doi.org/10.1021/ic400174r.

[66] J.D. Silversides, R. Smith, S.J. Archibald, Challenges in chelating positron emitting copper isotopes: tailored synthesis of unsymmetric chelators to form ultra stable complexes, Dalton Trans. 40 (2011) 6289, https://doi.org/10.1039/c0dt01395a.

[67] APEX3, Bruker AXS Inc, Madison, Wisconsin, USA, 2016.

[68] SAINT, Bruker AXS Inc, Madison, Wisconsin, USA, 2015.

[69] G.M. Sheldrick, SADABS, Bruker AXS Inc., Madison, Wisconsin, USA, 2014.

[70] G.M. Sheldrick, A short history of SHELX, Acta Crystallogr. A. 64 (2008) 112–122, https://doi.org/10.1107/S0108767307043930.

[71] G.M. Sheldrick, Crystal structure refinement with SHELXL, Acta Crystallogr. Sect. C, Struct. Chem. 71 (2015) 3–8, https://doi.org/10.1107/S2053229614024218.

[72] J. Dale, Exploratory calculations of medium and large rings, Acta Chem. Scand. 27 (1973) 1115–1129, https://doi.org/10.3891/acta.chem.scand.27-1115.

[73] M. Meyer, V. Dahaoui-Gindrey, C. Lecomte, R. Guilard, Conformations and coordination schemes of carboxylate and carbamoyl derivatives of the tetraazamacrocycles cyclen and cyclam, and the relation to their protonation states, Coord. Chem. Rev. 178–180 (1998) 1313–1405, https://doi.org/10.1016/S0010-8545(98)00169-6.

[74] R. Pujales-Paradela, T. Savić, I. Brandariz, P. Pérez-Lourido, G. Angelovski, D. Esteban-Gómez, C. Platas-Iglesias, Reinforced Ni(II)-cyclam derivatives as dual ^{1}H/ ^{19}F MRI probes, Chem. Commun. 55 (2019) 4115–4118, https://doi.org/10.1039/C9CC01204D.

[75] G.R. Weisman, E.H. Wong, D.C. Hill, M.E. Rogers, D.P. Reed, J.C. Calabrese, Synthesis and transition-metal complexes of new cross-bridged tetraamine ligands, Chem. Commun. (1996) 947, https://doi.org/10.1039/cc9960000947.

[76] W. Niu, E.H. Wong, G.R. Weisman, D.C. Hill, D.J. Tranchemontagne, K.-C. Lam, R.D. Sommer, L.N. Zakharov, A.L. Rheingold, Inside or outside a ligand cleft? Synthetic, structural, and kinetic inertness studies of zinc, cadmium, and mercury complexes of cross-bridged cyclam and cyclen, Dalton Trans. (2004) 3536, https://doi.org/10.1039/b410738a.

[77] D.G. Jones, K.R. Wilson, D.J. Cannon-Smith, A.D. Shircliff, Z. Zhang, Z. Chen, T. J. Prior, G. Yin, T.J. Hubin, Synthesis, structural studies, and oxidation catalysis of the late-first-row-transition-metal complexes of a 2-Pyridylmethyl pendant-armed ethylene cross-bridged Cyclam, Inorg. Chem. 54 (2015) 2221–2234, https://doi.org/10.1021/ic502699m.

[78] M. Pinsky, D. Avnir, Continuous symmetry measures. 5. The classical Polyhedra, Inorg. Chem. 37 (1998) 5575–5582, https://doi.org/10.1021/ic9804925.

[79] S. Alvarez, M. Llunell, Continuous symmetry measures of penta-coordinate molecules: berry and non-berry distortions of the trigonal bipyramid †, J. Chem. Soc. Dalton Trans. (2000) 3288–3303, https://doi.org/10.1039/b004878j.

[80] E.H. Wong, G.R. Weisman, D.C. Hill, D.P. Reed, M.E. Rogers, J.S. Condon, M. A. Fagan, J.C. Calabrese, K.-C. Lam, I.A. Guzei, A.L. Rheingold, Synthesis and characterization of cross-bridged Cyclams and pendant-armed derivatives and structural studies of their copper(II) complexes, J. Am. Chem. Soc. 122 (2000) 10561–10572, https://doi.org/10.1021/ja001295j.

[81] N. Camus, Z. Halime, N. Le Bris, H. Bernard, C. Platas-Iglesias, R. Tripier, Full control of the Regiospecific N -functionalization of C -functionalized Cyclam Bisaminal derivatives and application to the synthesis of their TETA, TE2A, and CB-TE2A analogues, J. Org. Chem. 79 (2014) 1885–1899, https://doi.org/10.1021/jo4028566.

[82] M.L. Moritz, Why 0.9% saline is isotonic: understanding the aqueous phase of plasma and the difference between osmolarity and osmolality, Pediatr. Nephrol. 34 (2019) 1299–1300, https://doi.org/10.1007/s00467-018-4084-2.

[83] B.C. Challis, L.F. Larkworthy, J.H. Ridd, Nitrosation, Diazotisation, and Deamination. Part X. * the acid-catalysed diazotisation of p-Nitroaniline and 2,4-Dinitroaniline in aqueous Perchloric acid (up to 3.0M), J. Chem. Soc. (1962) 5203–5207.

[84] A. Kriaa, N. Hamdi, K. Jbali, M. Tzinmann, Kinetics study of iron dissolution in highly concentrated acidic media using Hammett acidity function, Corros. Sci. 50 (2008) 3487–3493, https://doi.org/10.1016/j.corsci.2008.09.004.

[85] A.W. Addison, T.N. Rao, J. Reedijk, J. van Rijn, G.C. Verschoor, Synthesis, structure, and spectroscopic properties of copper(II) compounds containing nitrogen–Sulphur donor ligands; the crystal and molecular structure of aqua[1,7-bis(N-methylbenzimidazol-2′-yl)-2,6-dithiaheptane]copper(II) perchlorate, J Chem Soc Dalton Trans. (1984) 1349–1356, https://doi.org/10.1039/DT9840001349.

[86] V. Ji Ram, A. Sethi, M. Nath, R. Pratap, Five-membered heterocycles, in, Chem. Heterocycles, Elsevier (2019) 149–478, https://doi.org/10.1016/B978-0-08-101033-4.00005-X.

[87] A. Forgács, L. Tei, Z. Baranyai, I. Tóth, L. Zékány, M. Botta, A Bisamide derivative of [Mn(1,4-DO2A)] - solution thermodynamic, kinetic and NMR Relaxometric studies, Eur. J. Inorg. Chem. 2016 (2016) 1165–1174, https://doi.org/10.1002/ejic.201501415.

[88] A. Pasha, G. Tircsó, E.T. Benyó, E. Brücher, A.D. Sherry, Synthesis and characterization of DOTA-(amide)$_4$ derivatives: equilibrium and kinetic behavior of their lanthanide(III) complexes, Eur. J. Inorg. Chem. 2007 (2007) 4340–4349, https://doi.org/10.1002/ejic.200700354.

[89] Z. Garda, E. Molnár, F.K. Kálmán, R. Botár, V. Nagy, Z. Baranyai, E. Brücher, Z. Kovács, I. Tóth, G. Tircsó, Effect of the nature of donor atoms on the thermodynamic, kinetic and relaxation properties of Mn(II) complexes formed with some Trisubstituted 12-membered macrocyclic ligands, Front. Chem. 6 (2018) 232, https://doi.org/10.3389/fchem.2018.00232.

[90] U. Kreher, M.T.W. Hearn, B. Moubaraki, K.S. Murray, L. Spiccia, Coordination chemistry of 1,4-bis(carboxymethyl)-1,4,7-triazacyclononane: synthesis and characterization of mononuclear and binuclear μ-oxo-bridged iron(III) complexes,

and a 1D-helical copper(II) chain, Polyhedron. 26 (2007) 3205–3216, https://doi.org/10.1016/j.poly.2007.02.027.

[91] B.A. Vaughn, A.M. Brown, S.H. Ahn, J.R. Robinson, E. Boros, Is less more? Influence of the coordination geometry of copper(II) Picolinate chelate complexes on metabolic stability, Inorg. Chem. 59 (2020) 16095–16108, https://doi.org/10.1021/acs.inorgchem.0c02314.

[92] I. Voráčová, J. Vaněk, J. Pasulka, Z. Střelcová, P. Lubal, P. Hermann, Dissociation kinetics study of copper(II) complexes of DO3A, DOTA and its monosubstituted derivatives, Polyhedron. 61 (2013) 99–104, https://doi.org/10.1016/j.poly.2013.05.042.

[93] R. Ševčík, J. Vaněk, P. Lubal, Z. Kotková, J. Kotek, P. Hermann, Formation and dissociation kinetics of copper(II) complexes with tetraphosphorus acid DOTA analogs, Polyhedron. 67 (2014) 449–455, https://doi.org/10.1016/j.poly.2013.09.024.

[94] D. Zeng, Y. Guo, A.G. White, Z. Cai, J. Modi, R. Ferdani, C.J. Anderson, Comparison of conjugation strategies of cross-bridged macrocyclic chelators with Cetuximab for Copper-64 radiolabeling and PET imaging of EGFR in colorectal tumor-bearing mice, Mol. Pharm. 11 (2014) 3980–3987, https://doi.org/10.1021/mp500004m.

[95] Y. Kouzou, Volume changes and equilibrium constants for protonation of [M (edta)]$^{2-}$, Bull. Chem. Soc. Jpn. 58 (1985) 2778–2781, https://doi.org/10.1246/bcsj.58.2778.

[96] E.P. Friis, J.E.T. Andersen, L.L. Madsen, N. Bonander, P. Moller, J. Ulstrup, Dynamics of Pseudomonas aeruginosa azurin and its Cys3Ser mutant at single-crystal gold surfaces investigated by cyclic voltammetry and atomic force microscopy 43, 1998, pp. 1114–1122.

[97] N. Elgrishi, K.J. Rountree, B.D. McCarthy, E.S. Rountree, T.T. Eisenhart, J. L. Dempsey, A practical Beginner's guide to cyclic voltammetry, J. Chem. Educ. 95 (2018) 197–206, https://doi.org/10.1021/acs.jchemed.7b00361.

[98] M.M. Bernardo, M.J. Heeg, R.R. Schroeder, L.A. Ochrymowycz, D.B. Rorabacher, Comparison of the influence of saturated nitrogen and sulfur donor atoms on the properties of copper(II/I)-macrocyclic polyamino polythiaether ligand complexes: redox potentials and protonation and stability constants of CuIL species and new structural data, Inorg. Chem. 31 (1992) 191–198, https://doi.org/10.1021/ic00028a013.

[99] M. Regueiro-Figueroa, J.L. Barriada, A. Pallier, D. Esteban-Gómez, A. de Blas, T. Rodríguez-Blas, É. Tóth, C. Platas-Iglesias, Stabilizing divalent europium in aqueous solution using size-discrimination and electrostatic effects, Inorg. Chem. 54 (2015) 4940–4952, https://doi.org/10.1021/acs.inorgchem.5b00548.

[100] P. Bagchi, M.T. Morgan, J. Bacsa, C.J. Fahrni, Robust affinity standards for cu(I) biochemistry, J. Am. Chem. Soc. 135 (2013) 18549–18559, https://doi.org/10.1021/ja408827d.

[101] G. Salinas, J.G. Ibanez, R. Vásquez-Medrano, B.A. Frontana-Uribe, Analysis of cu in Mezcal commercial samples using square wave anodic stripping voltammetry, J. Electrochem. Sci. Technol. 9 (2018) 276–281, https://doi.org/10.33961/JECST.2018.9.4.276.

[102] J. Du, J.J. Cullen, G.R. Buettner, Ascorbic acid: chemistry, biology and the treatment of cancer, Biochim. Biophys. Acta BBA - Rev. Cancer. 2012 (1826) 443–457, https://doi.org/10.1016/j.bbcan.2012.06.003.

[103] C. Creutz, Complexities of ascorbate as a reducing agent, Inorg. Chem. 20 (1981) 4449–4452, https://doi.org/10.1021/ic50226a088.

[104] T. Matsui, Y. Kitagawa, M. Okumura, Y. Shigeta, Accurate standard hydrogen electrode potential and applications to the redox potentials of vitamin C and NAD/NADH, J. Phys. Chem. A 119 (2015) 369–376, https://doi.org/10.1021/jp508308y.

[105] E. Tutem, R. Apak, F. Baykut, Spectrophotometric determination of trace amounts of copper(I) and reducing agents with Neocuproine in the Presence of Copper(II) 116, 1991, pp. 89–94.

[106] Z. Xiao, J. Brose, S. Schimo, S.M. Ackland, S. La Fontaine, A.G. Wedd, Unification of the copper(I) binding affinities of the Metallo-chaperones Atx1, Atox1, and related proteins, J. Biol. Chem. 286 (2011) 11047–11055, https://doi.org/10.1074/jbc.M110.213074.

[107] B.S. Winkler, S.M. Orselli, T.S. Rex, The redox couple between glutathione and ascorbic acid: a chemical and physiological perspective, Free Radic. Biol. Med. 17 (1994) 333–349, https://doi.org/10.1016/0891-5849(94)90019-1.

[108] M.M. Taqui, A.E. Martell Khan, Metal ion and metal chelate catalyzed oxidation of ascorbic acid by molecular oxygen. II. Cupric and ferric chelate catalyzed oxidation, J. Am. Chem. Soc. 89 (1967) 7104–7111, https://doi.org/10.1021/ja01002a046.

[109] T. Akbıyık, İ. Sönmezoğlu, K. Güçlü, İ. Tor, R. Apak, Protection of ascorbic acid from copper(II)−catalyzed oxidative degradation in the presence of fruit acids: citric, oxalic, tartaric, malic, malonic, and Fumaric acids, Int. J. Food Prop. 15 (2012) 398–411, https://doi.org/10.1080/10942912.2010.487630.

[110] A.N. Laguta, S.V. Eltsov, N.O. Mchedlov-Petrossyan, Nitrophenol violet as a new tool for studying of kinetics of reactions in solutions, J. Chem. Educ. 98 (2021) 2964–2972, https://doi.org/10.1021/acs.jchemed.9b00115.

[111] J. Shen, P.T. Griffiths, S.J. Campbell, B. Utinger, M. Kalberer, S.E. Paulson, Ascorbate oxidation by iron, copper and reactive oxygen species: review, model development, and derivation of key rate constants, Sci. Rep. 11 (2021) 7417, https://doi.org/10.1038/s41598-021-86477-8.

[112] G.G. Manov, R.G. Bates, W.J. Hamer, S.F. Acree, Values of the constants in the Debye–Hückel equation for activity coefficients, J. Am. Chem. Soc. 65 (1943) 1765–1767.

[113] P.M. May, P.W. Linder, D.R. Williams, Computer simulation of metal-ion equilibria in biofluids: models for the low-molecular-weight complex distribution of calcium(II), magnesium(II), manganese(II), iron(III), copper(II), zinc(II), and

lead(II) ions in human blood plasma, J. Chem. Soc. Dalton Trans. (1977) 588, https://doi.org/10.1039/dt9770000588.

[114] Z. Baranyai, F. Carniato, A. Nucera, D. Horváth, L. Tei, C. Platas-Iglesias, M. Botta, Defining the conditions for the development of the emerging class of Fe^{III}-based MRI contrast agents, Chem. Sci. 12 (2021) 11138–11145, https://doi.org/10.1039/D1SC02200H.

[115] M.G. Basallote, C.E. Castillo, M.A. Máñez, P. Lubal, M. Martínez, C. Rodríguez, J. Vaněk, Striking medium effects on the kinetics of decomposition of macrocyclic Cu^{2+} complexes: additional considerations to be taken when designing Copper-64 radiopharmaceuticals, Inorg. Chem. Commun. 13 (2010) 1272–1274, https://doi.org/10.1016/j.inoche.2010.07.013.